
Thermal emission from isolated neutron stars: theoretical and observational aspects

Vyacheslav E. Zavlin

Space Science Laboratory, NASA Marshall Space Flight Center, SD59, Huntsville,
AL 35805, USA; vyacheslav.zavlin@msfc.nasa.gov

Summary. The possibility for direct investigation of thermal emission from isolated neutron stars was opened about 25 years ago with the launch of the first X-ray observatory *Einstein*. A significant contribution to this study was provided by *ROSAT* in 1990's. The outstanding capabilities of the currently operating observatories, *Chandra* and *XMM-Newton*, have greatly increased the potential to observe and analyze thermal radiation from the neutron star surfaces. Confronting observational data with theoretical models of thermal emission, presumably formed in neutron star atmospheres, allows one to infer the surface temperatures, magnetic fields, chemical composition, and neutron star masses and radii. This information, supplemented with model equations of state and neutron star cooling models, provides an opportunity to understand the fundamental properties of the superdense matter in the neutron star interiors. I review the current status and most important results obtained from modeling neutron star thermal emission and present selected *Chandra* and *XMM-Newton* results on thermal radiation from various types of these objects: ordinary radio pulsars with ages ranging from about 2 kyr to 20 Myr (J1119–6127, Vela, B1706–44, J0538+2817, B2334+61, B0656+14, B1055–52, Geminga, B0950+08, J2043+2740), millisecond pulsars (J0030+0451, J2124–3358, J1024–0719, J0437–4715), putative pulsars (CXOU j061705.3+222127, RX J0007.0+7302), central compact objects in supernova remnants (in particular, 1E 1207.4–5209), and isolated radio-quiet neutron stars.

1 Brief historical overview

Before the first neutron star was actually discovered as a radio pulsar¹ by Jocelyn Bell in 1967 (Hewish et al. 1968), it had been predicted that neutron stars, which are thought to represent the final stage of the stellar evolution, can be powerful sources of thermal X-ray emission just because these elusive objects are to be hot (Chiu & Salpeter 1964, Tsuruta 1964), in the literal (expected surface temperature $T_{\text{surf}} \sim 1$ MK) and a figurative sense. Remarkably, this idea and the discovery of the first pulsar became one of motivations for

¹ PSR B1919+21

further developing X-ray astronomy started at the end of 50's of the twentieth century. For objective reasons, I am not an expert on the history of X-ray astronomy, but I hope nobody would throw a stone at me for saying that the hunt for thermal emission from neutron stars began with the launch of the *Einstein* observatory in 1978. *Einstein* detected X-ray emission in the 0.2–4 keV range from a number of neutron stars and neutron star candidates (mainly as compact sources in supernova remnants [SNRs]). Of those, the well-known middle-aged radio pulsars B0656+14 and B1055-52 and the old pulsar B0950+08, which emit thermal X-ray radiation, are discussed in §4. The launch of the *ROSAT* mission sensitive in the 0.1-2.4 keV range opened a “decade of space science” in 1990's and provided a great contribution in observing X-ray emission from neutron stars. Speaking of which, the identification of the γ -ray source Geminga as a pulsar and, hence, a neutron star (Halpern & Holt 1992) is one of the major results achieved with *ROSAT*. Those were also supported by observations at energies up to 10 keV with the *ASCA* and *BeppoSAX* X-ray observatories, with the *EUVE* satellite covering the 0.07–0.2 keV range, as well as with *HST* in optical/*UV* range. Readers interested in more details on results from observations of neutron stars conducted in the last century can find them in the historical review by Becker & Pavlov (2001). New excellent observational data on neutron stars collected with two currently operating powerful X-ray missions, *Chandra* and *XMM-Newton* (both launched in 1999), provide a breakthrough in studying emission properties of these enigmatic objects. I do not know whether anyone has ever accurately counted the total number of *isolated* (i.e., nonaccreting) neutron stars of different types detected in X-rays, but I believe the number is at least sixty². Results from a significant fraction of these observations have been reviewed by Becker & Aschenbach (2002), Pavlov, Zavlin & Sanwal (2002), Kaspi, Roberts & Harding (2006), and Weisskopf et al. (2007).

2 Properties of X-ray emission from isolated neutron stars

Generally, X-ray radiation from an isolated³ neutron star can consist of two distinguished components: the nonthermal emission due to the pulsar activity and the radiation originating from the stellar surface. The nonthermal component is usually described by a power-law spectral model and attributed to radiation produced by synchrotron and/or inverse Compton processes in the pulsar magnetosphere, whereas the thermal emission can originate from either the entire surface of a cooling neutron star or small hot spots around the magnetic poles (polar caps) on the star surface, or both. The sketch shown in Figure 1 represents an evolutionary picture of these two radiative components expected in X-ray emission of neutron stars. In the majority of very

² As at the end of 2006.

³ The term “isolated” is omitted hereafter in the text.

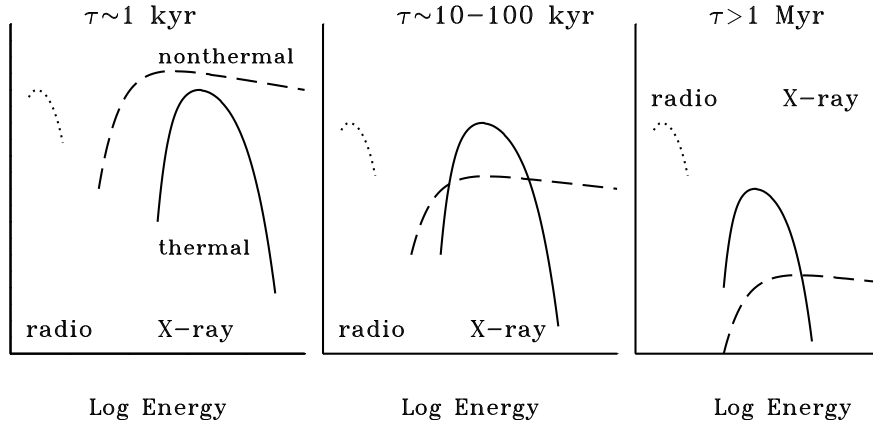


Fig. 1. Sketch illustrating what radiative component, nonthermal (dashes) or thermal (solid curves), is expected to dominate in X-ray flux of neutron stars of different ages τ (see § 2).

young pulsars ($\tau \sim 1$ kyr) the nonthermal component dominates (see the left panel in Fig. 1), making it virtually impossible to accurately measure the thermal flux; only upper limits on the surface temperature T_{surf} could be derived, as it was done for the famous Crab pulsar (Tennant et al. 2001) and PSR J0205+6449 in the SNR 3C 58 (Slane et al. 2004a). As a pulsar becomes older, its nonthermal luminosity decreases (roughly) proportional to its spin-down power $\dot{E} = 4\pi^2 IP^{-3}\dot{P}$ (I , P , and \dot{P} are the neutron star moment of inertia, spin period and its derivative, respectively), which is thought to drop with the star age τ , $\dot{E} \sim \tau^{-m}$, where $m \simeq 2-4$ (depending on the pulsar magneto-dipole braking index). On the other hand, the thermal luminosity of an aging and cooling neutron star decreases slower than the nonthermal one for ages $\tau \sim 10-100$ kyr, up to the end of the neutrino-cooling era ($\tau \sim 1$ Myr). Thus, the thermal radiation from the *entire* stellar surface can dominate at soft X-ray energies for *middle-aged pulsars* ($\tau \sim 100$ kyr) and some younger pulsars ($\tau \sim 10$ kyr). This situation is shown in the middle panel of Fig. 1. For neutron stars older than about 1 Myr, the surface temperature is too low, $T_{\text{surf}} \lesssim 0.1$ MK, to detect the thermal radiation from the whole surface in X-rays; only hot polar caps can be observable. As predicted by virtually all pulsar models, these polar caps can be heated up to X-ray temperatures (~ 1 MK) by relativistic particles generated in pulsar acceleration zones. A conventional assumption about the polar cap radius is that it is close to the radius within which open magnetic field lines originate from the pulsar surface, $R_{\text{pc}}^* = [2\pi R^3/cP]^{1/2} \simeq 0.5 [P/0.1 \text{ s}]^{-1/2}$ km (for a neutron star radius $R = 10$ km). As the spin-down power \dot{E} is the energy source for both nonthermal and thermal polar-cap components, it is hard to predict which of

them would prevail in X-ray flux of an old neutron star. However, it cannot be ruled out (and is proven by observations — see §4.5) that the thermal one may be dominant, as indicated in the right panel of Fig. 1. Remarkably, of neutron stars with detected X-ray emission, more than a half reveal thermal radiation. To interpret these observations, one needs reliable models of neutron star thermal emission. This paper reviews theoretical and observational aspects of studying thermal radiation from neutron stars.

3 Theoretical modeling of thermal radiation from neutron stars

There are a few questions to be answered before immersing into details on the theoretical modeling of neutron star thermal emission.

3.1 Why needed?

The main question is why studying the thermal emission is needed and interesting. Shortly, comparing observed thermal spectrum of a neutron star with theoretical models can allow one to infer the surface effective temperature T_{eff}^{∞} and total bolometric flux F_{bol}^{∞} (redshifted quantities, i.e., as measured by a distant observer) and estimate the actual (unredshifted) parameters, $T_{\text{eff}} = g_r^{-1} T_{\text{eff}}^{\infty}$ and $F_{\text{bol}} = g_r^{-2} F_{\text{bol}}^{\infty}$, where $g_r = [1 - 2GM/Rc^2]^{1/2}$ is the gravitational redshift determined by the neutron star mass M and radius R . If the distance to the neutron star, D , is known, then the measured temperature and flux yield the apparent (redshifted) radius of the star

$$R^{\infty} = D \left[\frac{F_{\text{bol}}^{\infty}}{\sigma_{\text{SB}} (T_{\text{eff}}^{\infty})^4} \right]^{1/2}, \quad (1)$$

where σ_{SB} is the Stefan-Boltzmann constant. This in turn links the actual neutron star radius and mass to each other via the relation $R^{\infty} = g_r^{-1} R$, or

$$M = \frac{c^2 R}{2G} \left[1 - \left(\frac{R}{R^{\infty}} \right)^2 \right]. \quad (2)$$

As seen in Figure 2, the latter puts constraints on equation of state of the superdense neutron star matter. Moreover, if one manages to measure the gravitational redshift of a neutron star, for example, via detecting and identifying spectral features in its X-ray flux, then it yields a unique solution for the neutron star mass and radius, and — Bingo! — the long-sought equation of state of the neutron star inner matter is found and the ultimate goal of the neutron star physics is achieved! (Un)fortunately, the real life is more complicated than it may seem. Anyway, even although solving the neutron star mystery seems to be far away, investigating thermal emission from

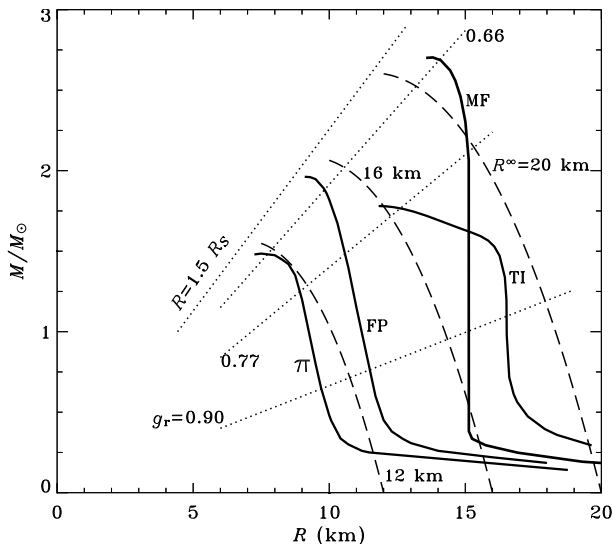


Fig. 2. Neutron star mass-radius diagram with lines of constant values of the gravitational parameter g_r (dots), redshifted radius $R^\infty = g_r^{-1}R$ (dashes) and four $M(R)$ relations (solid curves) corresponding to “hard” (MF and TI) and “soft” (π and FP) equations of state of superdense matter (see, e.g., Shapiro & Teukolsky 1983). The values of M and R for realistic equations of state lie below the straight line $R = 1.5R_S$ (or $g_r = 1/\sqrt{3}$), where $R_S = 2GM/c^2 = 2.95[M/M_\odot]$ km is the Schwarzschild radius.

these objects of different ages can trace their thermal evolution, that in turn sheds light on internal composition and nucleon superfluidity of the superdense matter (see Yakovlev et al. 2005 for a review). In addition, inferring surface properties of a neutron star (temperature, magnetic field, chemical composition) tells about its formation and interaction with environment.

3.2 More questions

Like in usual stars, thermal radiation of neutron stars is formed in the superficial (surface) layers. Hence, the next question is about the state of the neutron star surface. In principle, it can be in the gaseous state (atmosphere) or in a condensed state (liquid or solid), depending on surface temperature, magnetic field B and chemical composition. For instance, according to the estimates by Lai & Salpeter (1997), hydrogen is condensed in surface layers if $T_{\text{surf}} \lesssim 0.1$ MK at $B = 1 \times 10^{13}$ G and $T_{\text{surf}} \lesssim 1$ MK at $B = 5 \times 10^{14}$ G. At higher temperatures and/or lower magnetic fields, hydrogen does not condensate and forms an atmosphere. As the majority of known neutron stars seem to possess surface magnetic fields of $B \sim 10^{10}$ – 10^{12} G or less, they are expected to have an atmosphere. Therefore, below I mainly discuss properties of neutron star atmospheres.

The chemical composition affects not only the state of the surface, but it also determines the properties of emitted radiation. What would the composition of the stellar surface be? In case of neutron stars, one can expect that the emitting layers are comprised of just one, lightest available, chemical element because heavier elements sink into deeper layers due to the immense neutron star gravitation (Alcock & Illarionov 1980). For instance, even a small amount of hydrogen, with a surface density of $\sim 1 \text{ g cm}^{-2}$, is sufficient for the radiation to be indistinguishable from that emitted from a purely hydrogen atmosphere. Such an amount of hydrogen, $\sim 10^{-20} M_\odot$, can be delivered onto the neutron star surface by, e.g., (weak) accretion from the interstellar medium during the neutron star life and/or fallback of a fraction of the envelope ejected during the supernova explosion. If no hydrogen is present at the surface (e.g., because of diffuse nuclear burning — see Chang & Bildsten 2004), a heavier chemical element is responsible for the radiative properties of the neutron star atmosphere. However, a mixture of elements can be observed in the emitting layers if a neutron star is experiencing accretion with such a rate that the accreting matter is supplied faster than the gravitational separation occurs.

What else makes neutron star atmospheres very special? It is of course the enormous gravity at the neutron star surface, with typical gravitational acceleration $g \sim 10^{14}\text{-}10^{15} \text{ cm s}^{-2}$, and very strong, even huge, surface magnetic fields. The gravity makes the atmospheres very thin, with a typical thickness $H \sim kT_{\text{surf}}/[m_p g] \sim 0.1\text{-}10 \text{ cm}$ (k is the Boltzmann constant and m_p is proton mass), and dense, $\rho \sim 10^{-2}\text{-}10^2 \text{ g cm}^{-3}$. Such a high density causes strong nonideality effects (pressure ionization, smoothed spectral features) which must be taken into account (e.g., Pavlov et al. 1995). In addition, the strong gravitational field bends the photon trajectories near the neutron star surface (Pechenick, Ftaclas & Cohen 1983), as illustrated in Figure 3. This effect depends on the gravitational parameter g_r , and it can even make the whole surface visible if the neutron star is massive enough, $1.92 [10 \text{ km}/R] < [M/M_\odot] < 2.25 [10 \text{ km}/R]$. In particular, the gravitational bending strongly affects the observed pulsations of thermal emission (Zavlin, Shibano & Pavlov 1995). As shown by Pavlov & Zavlin (1997) and Zavlin & Pavlov (1998, 2004a), analyzing pulsed thermal radiation can put constraints on the mass-to-radius ratio, M/R , and the neutron star geometry (orientation of spin and magnetic axes with respect to each other and direction to a distant observer — see Fig. 3).

Huge magnetic fields, up to $B \sim 10^{14} \text{ G}$, expected in the surface layers of neutron stars change the properties of the atmospheric matter and the emergent radiation very drastically. Strongly magnetized atmospheres are essentially anisotropic, with radiative opacities depending on the magnetic field and the direction and polarization of radiation. Moreover, since the ratio of the cyclotron energy, $E_{ce} = \hbar e B / m_e c$, to the Coulomb energy is very large (e.g., $\beta \equiv E_{ce}/[1 \text{ Ry}] = 850 [B/10^{12} \text{ G}]$ for a hydrogen atom), the structure of atoms is strongly distorted by the magnetic field. For instance, the binding

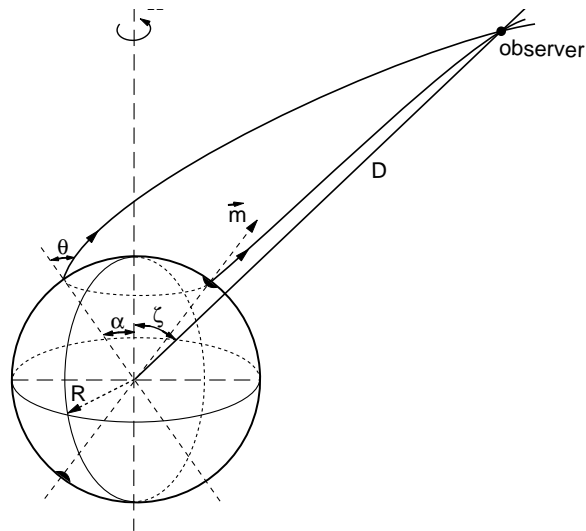


Fig. 3. Sketch illustrating bending of photon trajectories near the surface of a neutron star with spin, Ω , and magnetic, \mathbf{m} , axes. Black spots around the magnetic poles indicate possible heated polar caps on the star surface.

(ionization) energies of atoms are increased by a factor of $\sim \ln^2 \beta$ (e.g., the ionization potential of a hydrogen atom is about 0.3 keV at $B = 10^{13}$ G). This in turn significantly modifies ionization equilibrium of the neutron star atmospheric plasma. Another important effect is that the heat conductivity of the neutron star crust is anisotropic, being higher along the magnetic field. This results in a nonuniform surface temperature distribution (Greenstein & Hartke 1983), which leads to pulsations of the thermal radiation due to neutron star rotation.

Depending on the magnetic field strength, models of neutron star atmospheres are differentiated in two groups, “nonmagnetic” and “strongly magnetized”. The nonmagnetic models are constructed for $B \lesssim 10^9$ G, when the electron cyclotron energy, $E_{ce} \lesssim 0.01$ keV, is lower than the binding energy of atoms and thermal energy of particles, $E \sim kT_{\text{surf}}$. As a result, the effect of the magnetic field on the radiative opacities and emitted spectra is negligible at X-ray energies, $E \gtrsim 0.1$ keV. These models, constructed assuming $B = 0$ G, can be applicable to, for example, millisecond pulsars and neutron star transients in quiescence (e.g., Rutledge et al. 1999, 2001a,b and 2002), whereas magnetized models are intended mostly for radio pulsar with $B \sim 10^{10} - 10^{14}$ G. Below I summarize main results obtained from these two groups of neutron star atmosphere models. More details can be found in the extended review by Zavlin & Pavlov (2002).

3.3 Nonmagnetic atmosphere models

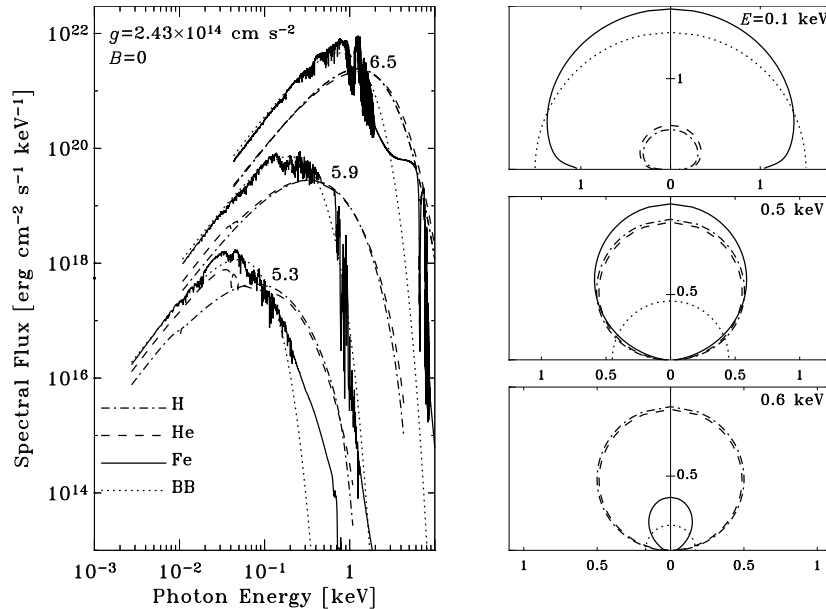


Fig. 4. *Left:* Spectra of emergent radiation for pure hydrogen, helium, and iron nonmagnetic atmospheres with different effective temperatures (numbers near the curves label $\text{Log } T_{\text{eff}}$ [T_{eff} in K]). ‘BB’ stands for blackbody spectrum. *Right:* Polar diagrams of normalized spectral specific intensities at different photon energies, E , and $\text{Log } T_{\text{eff}} = 5.9$, and for the same chemical compositions. The normal to the surface is directed upward.

Modeling nonmagnetic neutron star atmospheres was started in the pioneering work by Romani (1987). Since then, models for various surface chemical compositions have been developed by Rajagopal & Romani (1996), Zavlin, Pavlov & Shibano (1996), Zavlin et al. (1996), Werner & Deetjen (2000), Pavlov & Zavlin (2000a), Pons et al. (2002), Gänsicke, Braje & Romani (2002), and Heinke et al. (2006).

The general approach of the atmosphere modeling is as follows. Very small thickness of a neutron star atmosphere, $H \ll R \approx 10$ km (§ 3.2), allows one to use the plane-parallel (one-dimensional) approximation. In addition, because of rather high densities of the surface layers, the atmospheres are expected to be in the local thermodynamic equilibrium. The atmosphere modeling involves solving three main equations. The first one is the radiative transfer equation for the specific spectral intensity I_ν (e.g., Mihalas 1978):

$$\mu \frac{d}{dy} I_\nu = k_\nu (I_\nu - S_\nu), \quad (3)$$

where ν is photon frequency, μ is cosine of the angle θ between the normal to the surface and the wave-vector of outgoing radiation, y is the column density ($dy = \rho dz$, with z being the geometrical depth), $k_\nu = \alpha_\nu + \sigma_\nu$ is the total radiative opacity which includes the absorption, α_ν , and scattering, σ_ν , opacities, $S_\nu = (\sigma_\nu J_\nu + \alpha_\nu B_\nu) k_\nu^{-1}$ is the source function, $J_\nu = \frac{1}{2} \int_{-1}^1 I_\nu d\mu$ is the mean spectral intensity, and B_ν is the Planck function. The boundary condition for this equation is $I_\nu = 0$ for $\mu < 0$ at $y = 0$, assuming no incident radiation at the surface (valid at $R > 1.5R_S$ — see Fig. 2).

The atmospheres are supposed to be in radiative and hydrostatic equilibrium. The first condition implies that the total energy flux through the atmosphere is constant and transferred solely by radiation (electron heat conduction and convection are of no importance for typical parameters of interest),

$$\int_0^\infty d\nu \int_{-1}^1 \mu I_\nu d\mu = \sigma_{\text{SB}} T_{\text{eff}}^4. \quad (4)$$

The second condition means that the atmospheric pressure is $p = gy$ (the radiative force is insignificant unless $T_{\text{eff}} \gtrsim 10$ MK). Finally, these three equations are supplemented with the equation of state for the atmospheric plasma and equations of ionization equilibrium. The latter is needed for computing the electron number density and the fractions of ions in different stages of ionization to obtain the radiative opacity with account for free-free, bound-free and bound-bound transitions.

The main results of the atmosphere modeling are the properties of the emergent radiation demonstrated in Figure 4. The left panel of Fig. 4 presents the spectral fluxes of emergent radiation at a local surface point, $F_\nu = \int_0^1 \mu I_\nu d\mu$ (at $y = 0$), for several effective temperatures and chemical compositions (pure hydrogen, helium, and iron), together with blackbody spectra at the same values of T_{eff} . The atmosphere model spectra differ substantially from the blackbody ones, particularly in high-energy tails of the radiation from the light-element (hydrogen and helium) atmospheres. The reason is in the combination of two effects: rapid decrease of the light-element opacities with energy, $k_\nu \sim E^{-3}$, and temperature growth in the surface layers, $T(y)$, with depth y . Hence, the high-energy radiation is formed in deeper and hotter layers, with $T > T_{\text{eff}}$. The spectra emitted from the heavy-element atmospheres (see also Zavlin & Pavlov 2002 for spectra of solar-mixture compositions) exhibit numerous spectral lines and photoionization edges (e.g., M, L, and K spectral complexes in the iron spectra, at about 0.1, 0.8, and 7.1 keV, respectively) produced by ions in various ionization stages. Generally, they are closer to the blackbody radiation because the energy dependence of the heavy-element opacities is, on average, flatter than that for the light elements.

Although the opacity of the atmospheric plasma is isotropic in the non-magnetic case, the emitted radiation show substantial anisotropy, i. e., the specific intensity I_ν depends on the direction of emission due to the limb-darkening effect (see the right panel in Fig. 4): the larger angle θ between the

normal to the surface and direction of a specific intensity is, the longer path throughout the surface layers emerging photons travel to escape, and, hence, the stronger absorption the intensity undergoes. The anisotropy depends on photon energy and chemical composition of the atmosphere. This effect should be taken into account to model thermal radiation from a nonuniform neutron star surface.

The emergent radiation depends also on the surface gravity: a stronger gravitational acceleration increases the density of the atmospheric plasma, changes temperature run $T(y)$ and enhances the nonideality effects, which results in weaker (more smoothed) spectral features. The hardness of the spectral Wien tail at higher photon energies also alters with varying surface gravity because of the changes in the atmosphere structure (Zavlin, Pavlov & Shibano 1996, Heine et al. 2006). However, these effects are rather subtle and may be important only for analyzing observational data of extremely good statistics.

3.4 Magnetized atmosphere models

First magnetized hydrogen models have been developed by Shibano et al. (1992), Pavlov et al. (1994), Shibano & Zavlin (1995), Pavlov et al. (1995), and Zavlin et al. (1995). These models used simplified radiative opacities of strongly magnetized, partially ionized plasma, which did not include the bound-bound transitions. However, they are considered to be reliable enough in the case of high temperatures, $T_{\text{eff}} \approx 1$ MK, at typical pulsar fields, $B \sim 10^{12}$ G, when the atmospheric plasma is almost fully ionized even in the strong magnetized fields. Later on, completely ionized hydrogen models for superstrong magnetic fields, $B \sim 10^{14}$ – 10^{15} G, have been presented in a number of papers (Bezchastnov et al. 1996, Özel 2001, Ho & Lai 2001, Zane et al. 2001, Ho & Lai 2003), concerned mainly with the vacuum polarization effects first discussed by Pavlov & Gnedin (1984) and the proton cyclotron lines whose energies shift into the X-ray band at $B \gtrsim 2 \times 10^{13}$ G. Ho et al. (2003) presented models for partially ionized hydrogen atmospheres with magnetic fields up to 5×10^{14} G and effective temperatures down to about 0.5 MK. This work showed that the vacuum polarization affects not only the proton cyclotron line but also it suppresses spectral features caused by bound species, making them virtually unobservable in thermal spectra of strongly magnetized neutron stars. First set of magnetized atmospheres with a heavy-element composition (pure iron) was constructed by Rajagopal, Romani & Miller (1997), with the use of a rather crude approximations for the very complicated properties of iron ions in strong magnetic fields. Recently, a next step in modeling magnetized heavy-element (carbon, oxygen, neon) atmospheres with $B = 10^{12}$ – 10^{13} G and $T_{\text{eff}} = (1\text{--}5)$ MK has been undertaken by Mori & Ho (2006). These models imply latest developments in atomic physics and radiative opacities in strong magnetic fields (Mori & Hailey 2002, 2006). Like in the nonmagnetic case, the magnetized heavy-element atmo-

sphere emission shows many prominent spectral features which, if observed in real X-ray observational data, could be very useful to measure the neutron star magnetic field and mass-to-radius ratio, M/R .

All the above-mentioned works used the same approach for constructing magnetized atmosphere models, which is generally similar to the nonmagnetic case. The main difference is that the atmospheric radiation is polarized, and the radiative opacities depend on the polarization and direction of radiation. Gnedin & Pavlov (1974) described the radiative transfer in a strongly magnetized plasma in terms of coupled equations for specific intensities of two normal modes, $I_{\nu,1}$ and $I_{\nu,2}$, with different polarizations and opacities:

$$\mu \frac{d}{dy} I_{\nu,j}(\mathbf{n}) = k_{\nu,j}(\mathbf{n}) I_{\nu,j}(\mathbf{n}) - \left[\sum_{i=1}^2 \oint d\mathbf{n}' I_{\nu,i}(\mathbf{n}') \sigma_{\nu,ij}(\mathbf{n}', \mathbf{n}) + \alpha_{\nu,j}(\mathbf{n}) \frac{B_\nu}{2} \right], \quad (5)$$

where \mathbf{n} is the (unit) wave-vector, $\alpha_{\nu,j}$ is the absorption opacity for the j -th mode, $\sigma_{\nu,ij}$ is the scattering opacity from mode i to mode j , and $k_{\nu,j} = \alpha_{\nu,j} + \sum_{i=1}^2 \oint d\mathbf{n}' \sigma_{\nu,ij}(\mathbf{n}', \mathbf{n})$ is the total opacity. It should be noted that the opacity depends on the angle between the wave-vector and the magnetic field, so that I_ν depends not only on θ but also on Θ_B , the angle between the local magnetic field and the normal to the surface element. Similar to the nonmagnetic case, Eqs. (5) are supplemented with the equations of hydrostatic and radiative equilibrium (for the latter, Eq. [4] applies with $I_\nu = I_{\nu,1} + I_{\nu,2}$).

To deal with the problems caused by the sharp angular dependence of the radiative opacities (Kaminker, Pavlov & Shibano 1982), a two-step method for modeling of magnetic neutron star atmospheres was developed (Pavlov et al. 1994; Shibano & Zavlin 1995). At the first step, the radiative transfer is solved in the diffusion approximation for the mean intensities $J_{\nu,j} = (4\pi)^{-1} \oint I_{\nu,j}(\mathbf{n}) d\mathbf{n}$:

$$\frac{d}{dy} d_{\nu,j} \frac{d}{dy} J_{\nu,j} = \bar{\alpha}_{\nu,j} \left[J_{\nu,j} - \frac{B_\nu}{2} \right] + \bar{\sigma}_\nu [J_{\nu,j} - J_{\nu,3-j}], \quad (6)$$

where $\bar{\alpha}_{\nu,j} = (4\pi)^{-1} \oint d\mathbf{n} \alpha_{\nu,j}(\mathbf{n})$ and $\bar{\sigma}_\nu = (4\pi)^{-1} \oint \oint d\mathbf{n} d\mathbf{n}' \sigma_{\nu,12}(\mathbf{n}, \mathbf{n}')$ are the angle-averaged absorption and scattering opacities. The diffusion coefficient is $d_{\nu,j} = d_{\nu,j}^p \cos^2 \Theta_B + d_{\nu,j}^o \sin^2 \Theta_B$, with $d_{\nu,j}^p = \int_0^1 \mu^2 k_{\nu,j}^{-1} d\mu$ and $d_{\nu,j}^o = \int_0^1 (1-\mu^2) k_{\nu,j}^{-1} d\mu$. Next, the atmospheric structure obtained at the first step is corrected using an iterative procedure applied to the exact equations of the radiative transfer. Finally, the emergent intensity (at $y = 0$) is

$$I_{\nu,j} = \mu^{-1} \int_0^\infty \left[\alpha_{\nu,j} \frac{B_\nu}{2} + \sum_{i=1}^2 \sigma_{\nu,ij} J_{\nu,i} \right] \exp \left[-\nu^{-1} \int_0^y k_{\mu,j} dz \right] dy, \quad (7)$$

and the emitted spectral flux is computed as $F_\nu = \int_0^1 \mu \sum_{i=1}^2 I_{\nu,i} d\mu$. More details on the modeling of magnetized atmospheres can be found in Pavlov et al. (1995).

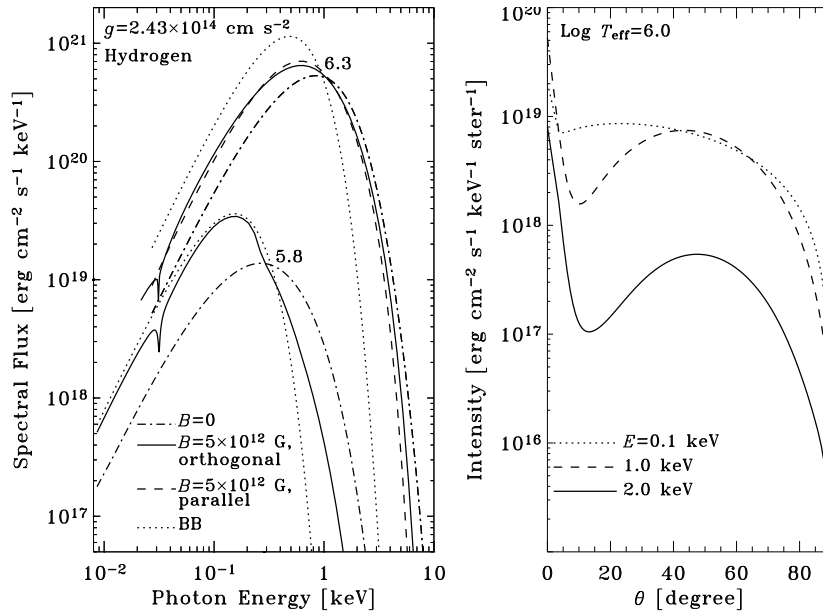


Fig. 5. *Left:* Spectra of radiation emergent from neutron star atmospheres for a magnetic field orthogonal and parallel to the surface with different effective temperatures (numbers near the curves label $\text{Log } T_{\text{eff}}$ [T_{eff} in K]). ‘BB’ stands for blackbody spectrum. *Right:* Dependences of specific intensities on the angle between the photon wave-vector and the magnetic field directed along the surface normal.

Figure 5 (left panel) shows polarization-summed spectral fluxes of the emergent radiation, F_ν , emitted by a local element of the neutron star surface, for two values of effective temperature and two magnetic field orientations, perpendicular and parallel to the surface ($\Theta_B = 0$ and 1, respectively). The main result is that the magnetized atmosphere spectra are harder than the blackbody radiation of the same T_{eff} , although they are softer than the nonmagnetic spectra. Similar to the nonmagnetic case, this is explained by the temperature growth with depth and the opacity decrease at higher energies, which is more gradual ($\propto E^{-1}$ for the mode with smaller opacity) in the magnetized plasam. At lower effective temperatures, $T_{\text{eff}} \lesssim 1$ MK, the photoionization opacity (due to bound-free transitions) becomes important, that affects the shape of emitted spectra (see the example with $\text{Log } T_{\text{eff}} = 5.8$ in Fig. 5). The proton cyclotron lines are seen at energies $E = 6.3 (B/10^{12} \text{ G})$ eV. If the magnetic field is very large, $B \gtrsim 10^{14}$ G, the proton cyclotron line shifts into the X-ray band. On the other hand, if the magnetic field is not so large,

$B = 10^{10}$ – 10^{12} G, the neutron star atmosphere spectra may exhibit the electron cyclotron lines in the X-ray band, at $E_{ce} = 11.6 (B/10^{12} \text{ G}) \text{ keV}$. Calculations of hydrogen atmosphere models which include bound-bound transitions (Zavlin & Pavlov 2002, Ho et al. 2003) show that spectral lines, considerably broadened by the motional Stark effect (Pavlov & Mészáros 1993, Pavlov & Potekhin 1995) may emerge at $T_{\text{eff}} \lesssim 0.5 \text{ MK}$. The strongest line corresponds to the transition between the ground state and the lowest excited state; its energy is $E \approx [75 + 0.13 \ln(B/10^{13} \text{ G}) + 63(B/10^{13} \text{ G})] \text{ eV}$.

Radiation emerging from a magnetized atmosphere is strongly anisotropic. Angular dependences of the local specific intensities, $I_\nu = I_{\nu,1} + I_{\nu,2}$ (Eq. [7]), show a complicated “pencil-plus-fan” structure — a narrow peak along the direction of the magnetic field (where the atmospheric plasma is most transparent for the radiation), and a broader peak at intermediate angles. The widths and strengths of the peaks depend on magnetic field and photon energy (see examples in the right panel of Fig. 5). Obviously, it is very important to account for this anisotropy while modeling the radiation from a neutron star with nonuniform surface magnetic field and effective temperature.

3.5 Thermal radiation as detected by a distant observer

Results presented in §§ 3.3 and 3.4 describe spectral radiation emitted by a *local* element at the neutron star surface. The effective temperature and/or magnetic field distributions over the surface can be nonuniform (for example, if a neutron star has a dipole magnetic field, the effective temperature decreases from the magnetic poles to the equator). To calculate the *total* emission, one has to integrate the local intensities, computed for local temperatures and magnetic fields, over the visible part of the surface S , with account for the gravitational redshift and bending of photon trajectories:

$$F(E_{\text{obs}}) = g_r \frac{1}{D^2} \int_S \mu I(E_{\text{obs}}/g_r) dS, \quad (8)$$

where $E_{\text{obs}} = g_r E$ is the observed (redshifted) photon energy. To take into account the interstellar absorption, a factor, $\exp[-n_{\text{H}} \sigma_{\text{eff}}(E)]$, should be added in Eq. (8) ($\sigma_{\text{eff}}[E]$ is the absorption cross section per hydrogen atom). More details about the integration over the neutron star surface can be found in Pavlov & Zavlin (2000b). It is worthwhile to mention that if a neutron star has a nonuniform distribution of the magnetic field, the integration broadens the spectral features. In addition, if a neutron star is a fast rotator, one should take into account the Doppler shifts of energies of photons emitted from surface elements moving with different radial velocities. Maximum values of these velocities, $v_r = 2\pi R P^{-1} \sin \zeta$ (ζ is the inclination of the rotation axis with respect to observer’s line of sight — see Fig. 3), can be as high as 10%–15% of the speed of light for millisecond periods. For instance, Zavlin & Pavlov (2002) showed that a fast rotation, $P \lesssim 10 \text{ ms}$, may lead to complete smearing

of weak and narrow spectral lines, provided $\sin \zeta$ is large enough, leaving only most prominent spectral jumps around the strongest photoionization edges.

If thermal radiation originated from small polar caps on the neutron star surface, it greatly simplifies Eq. (8):

$$F(E) = g_r \frac{S_a}{D^2} I(E/g_r, \theta^*), \quad (9)$$

where the apparent spot area S_a and the angle θ^* between the wave-vector of escaping radiation and the radius-vector to the hot spot are computed with account for the effect of gravitational bending. These quantities depend on the angles α (between the rotational and magnetic axes) and ζ (Fig. 3), and the gravitational parameter g_r (see Zavlin, Shibano & Pavlov 1995 for details).

The flux given by Eqs. (7) or (8) varies with the period of neutron star rotation. One can obtain a large variety of pulse profiles at different assumptions on the angles α and ζ and the neutron star mass-to-radius ratio. Examples of pulse profiles computed for radiation from the entire neutron star surface are shown in Zavlin & Pavlov (2002), whereas pulse profiles of thermal radiation from heated polar caps are presented by Zavlin, Shibano & Pavlov (1995) and Zavlin & Pavlov (2004a) for magnetized atmosphere models, and by Zavlin & Pavlov (1998) for nonmagnetic ones.

3.6 Atmosphere emission vs. blackbody radiation

Although the model atmosphere spectra are different from the blackbody radiation, very often an observed thermal spectrum can be fitted equally well with the blackbody and neutron star atmosphere models (see examples in § 4), particularly when the energy resolution is low and/or the energy band is narrow and/or observational data are of a poor quality. However, the parameters obtained from such fits are quite different, especially when the hydrogen or helium atmospheres are used. Since the light-element atmosphere spectra are much harder than the blackbody spectra at the same effective temperature, atmosphere model fits result in temperatures T_{atm} significantly lower than the blackbody temperature T_{bb} , with a typical ratio $T_{\text{bb}}/T_{\text{atm}} \sim 2-3$. On the other hand, to provide the same total energy flux, the blackbody fit yields a smaller normalization factor, proportional to S/D^2 (see Eq. [7]), than the atmosphere model fit does. In other words, the light-element atmosphere fit gives a considerably larger size of the emitting region, $S_{\text{atm}}/S_{\text{bb}} \sim 50-200$, for the same distance to the source. Note however that both neutron star atmosphere and blackbody models yield about the same values of bolometric luminosity $L_{\text{bol}}^\infty = g_r^2 L_{\text{bol}}$ as measured by a distant observer.

It is also worth to remember that blackbody radiation is *isotropic* and, hence, it results in weak pulsations of model flux, with a typical pulsed fraction around a few percents only.

Finally, the atmosphere models discussed here, both nonmagnetic and magnetized, are available for analyzing thermal X-ray emission observed from

neutron stars as a part of the X-ray Spectral Fitting Package⁴ (codes ‘NSA’ and ‘NSAGRAV’ in XSPEC) provided by the NASA’s High Energy Astrophysics Science Archive Reserach Center.

3.7 Modeling radiation from condensed neutron star surface

As mentioned above, if magnetic field of the neutron star surface is strong enough and the surface temperature is rather low, then the outermost surface layers could be in any state other than gaseous. For example, at $B = 10^{14}$ G and $T_{\text{surf}} \lesssim 0.5$ MK and $T_{\text{surf}} \lesssim 2$ MK for hydrogen and iron compositions, respectively, the surface would be in a condensed (solid) state (van Adelsberg et al. 2005). First models of thermal radiation emitted by condensed surface of a netron star were constructed by Turolla, Zane & Drake (2004) and van Adelsberg et al. (2005). These works showed that the overall spectral shape of X-ray flux emitted by a condensed surface is mostly featureless (only weak spectral features associated with ion cyclotron and electron plasma frequencies can appear in some cases) and fairly close to blackbody spectrum of the same temperature. The main difference between these two model spectra is that, because of suppressed emissivity of condensed surface, the surface radiation is reduced from the blackbody one by a factor of a few. Hence, applying condensed surface models to observed thermal emission is expected to result in temperature estimates close to and flux normalizations (proportional to the factor $[R^\infty/D]^2$) larger by a factor of few than those yielded by blackbody radiation.

4 Thermal emission from neutron stars: observational results

As already mentioned in § 2, thermal emission has been observed from a rather large number of neutron stars of different types. The majority of them is radio pulsars of different ages ranging from very young neutron stars to old and very old (millisecond) ones. In addition to active pulsars, a number of radio-quiet neutron stars emitting only thermal-like X-rays have been detected, with typical temperatures ~ 0.5 –5 MK. They are usually subdivided in four classes: Anomalous X-ray Pulsars (AXPs; Mereghetti et al. 2002, Kaspi 2006), Soft Gamma-ray Repeaters (SGRs; Kaspi 2004), “dim” or “truly isolated” radio-quiet neutron starss (i.e., not associated with SNRs; Haberl 2007) and compact central sources (CCOs) in SNRs (Pavlov et al. 2002, Pavlov, Sanwal & Teter 2004) which have been identified with neither active pulsars nor AXPs/SGRs. Observational manifestations (particularly, multiwavelength spectra) of radio-quiet neutron stars are quite different from those of active pulsars, and their properties have not been investigated as extensively, but the presence of the

⁴ <http://heasarc.gsfc.nasa.gov/docs/xanadu/xspec/>

thermal component in their radiation provides a clue to understand the nature of these objects. While the paper by Pavlov, Zavlin & Sanawal (2002) provides a detailed review on thermal emission from neutron stars, here I discuss a few most interesting and illustrative examples, concentrating mainly on spectral properties of detected thermal emission.

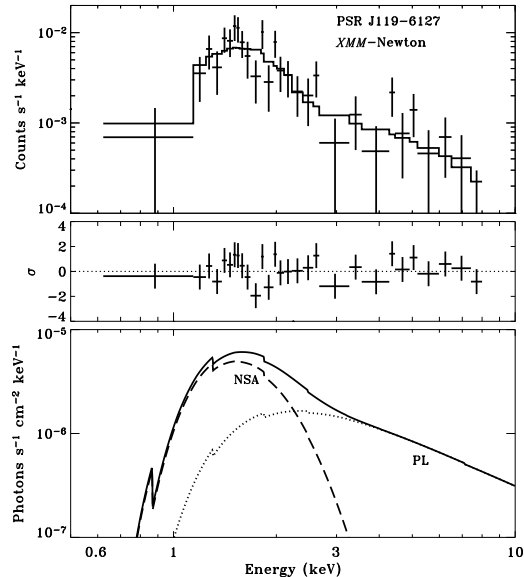


Fig. 6. Two-component, hydrogen magnetized atmosphere (NSA) model plus power law (PL), fit to the X-ray spectrum of PSR J1119–6127 detected with *XMM-Newton* (upper panel). The middle panel shows residuals in the fit, whereas the lower panel presents the contributions (attenuated by interstellar absorption) from the thermal (dashes) and nonthermal (dots) components (see § 4.1).

4.1 PSR J1119-6127

It is the youngest⁵, $\tau_c = 1.6$ kyr, and very energetic in terms of the spin-down power, $\dot{E} = 2.3 \times 10^{36}$ ergs s⁻¹, radio pulsar whose X-ray flux reveals a strong thermal component. The best representation of the pulsar’s spectrum detected with *XMM-Newton* is a two-component, thermal plus nonthermal, model (Gonzalez et al. 2005). The nonthermal emission dominating at energies $E \gtrsim 2.5$ keV is well fitted with a power-law spectrum of a photon index $\Gamma \simeq$

⁵ The characteristic age, $\tau_c = P/(2\dot{P})$, is a standard age estimate for the vast majority of radio and X-ray pulsars. Note however that it may be very inaccurate (see § 4.3).

1.5 and X-ray luminosity $L^{\text{nonth}} \simeq 0.8 \times 10^{33}$ ergs s^{-1} in the 0.2–10 keV range⁶. The thermal component can be fitted with a blackbody spectrum of an apparent (redshifted, see § 3.1) temperature $T_{\text{bb}}^{\infty} \simeq 2.4$ MK and radius $R_{\text{bb}}^{\infty} \simeq 3.4$ km (for the estimated distance⁷ to the pulsar $D = 8.4$ kpc), implying the measured bolometric luminosity $L_{\text{bol}}^{\infty} \simeq 2.7 \times 10^{33}$ ergs s^{-1} . This model fit would mean that the thermal radiation originates from a small hot area on the pulsar’s surface (polar caps?), although the inferred radius of the emitting area significantly exceeds the canonical radius $R_{\text{pc}}^* \simeq 0.2$ km predicted by theoretical models for PSR J1119–6127 with a spin period $P = 0.408$ s (see § 2). Alternatively, the thermal component can be interpreted as X-ray flux of an effective (actual) temperature $T_{\text{eff}} \simeq 1.6$ MK (or $T_{\text{eff}}^{\infty} = g_{\text{r}}^{-1} T_{\text{eff}} \simeq 1.2$ MK) emitted from the whole pulsar’s surface covered with a magnetized ($B \approx 1 \times 10^{13}$ G) hydrogen atmosphere⁸ (assuming the standard neutron star mass $M = 1.4 M_{\odot}$ and radius $R = 10$ km), yielding $L_{\text{bol}} \simeq 4.7 \times 10^{33}$ ergs s^{-1} (or $L_{\text{bol}}^{\infty} = g_{\text{r}}^2 L_{\text{bol}} \simeq 2.8 \times 10^{33}$ ergs s^{-1} , very close to the value obtained in the blackbody fit). In this interpretation, the parameters of the nonthermal component are virtually the same as those in the fit with the blackbody radiation. The best fit with the magnetized atmosphere model and power-law spectrum is shown in Figure 6.

Very importantly, the X-ray flux of PSR J1119–6127 detected in the 0.6–2 keV range, where the thermal component dominates, is pulsed, with a very large pulsed fraction, $f_{\text{p}} \approx 75\%$ (Conzalez et al. 2005). It should be noted that because of the strong gravitational bending effect (§ 3.2) such pulsations can be reconciled with neither (isotropic) blackbody radiation nor atmospheric emission from an *uniform* surface. On the other hand, no pulsations have been detected at energies $E > 2$ keV, that is rather a surprising result as nonthermal emission is expected to be strongly pulsed, especially that emitted by young and energetic pulsars.

The example of PSR J1119-6127 is remarkable in the sense that the situation with observing thermal emission from very young and active pulsars is not in fact as “pessimistic” as it may follow from the general picture described in § 2, and more such detections can be expected in future.

4.2 The Vela pulsar and PSR B1706-44

The superb angular resolution of *Chandra* made it possible to separate X-ray flux of the famous Vela pulsar ($P = 0.089$ s, $\tau_{\text{c}} = 11$ kyr, $\dot{E} = 6.9 \times 10^{36}$ ergs s^{-1}) from its bright pulsar-wind nebula and study the properties of the pulsar’s emission (Pavlov et al. 2001). The *Chandra* observations revealed

⁶ This energy range is used for all other estimates on L^{nonth} given in this work.

⁷ Distances cited in § 4 are either those estimated to SNRs which host some of discussed objects or derived from pulsar parallaxes or dispersion measures.

⁸ Note that the parameters of the atmosphere model cited in this work differ from those given in Gonzalez et al. (2005).

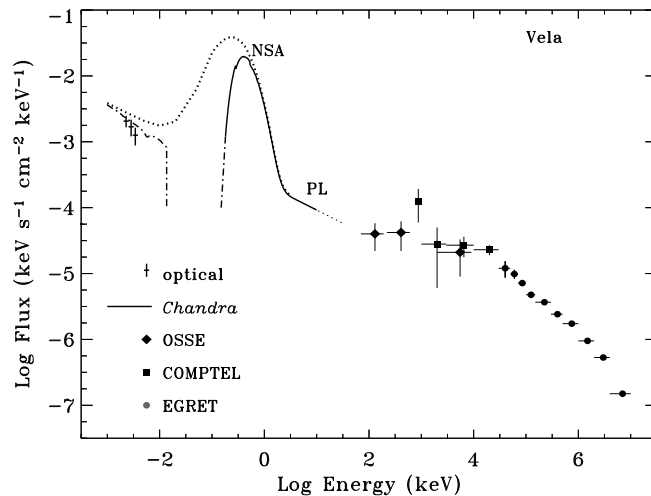


Fig. 7. Multiwavelength spectrum of the Vela pulsar detected with different missions. The solid line shows the X-ray spectrum obtained with *Chandra* and fitted with a two-component, neutron star atmosphere (NSA) and power-law (PL), model (see § 4.2). Dots correspond to the unabsorbed model spectrum. The dash-dotted lines show the extrapolated optical and EUV absorbed spectra.

that the bulk of the X-ray flux detected from Vela is of a thermal origin, and nonthermal emission dominates only at energies $E \gtrsim 2$ keV, similar to the case of PSR J1119–6127. The thermal component can be described equally well with either a blackbody spectrum or a magnetized ($B \approx 5 \times 10^{12}$ G) hydrogen⁹ atmosphere model. However, the parameters of the thermal component are significantly different in the blackbody and atmosphere model fits: $T_{\text{bb}}^{\infty} \simeq 1.6$ MK and $R_{\text{bb}}^{\infty} \simeq 2.8$ km, $T_{\text{eff}} \simeq 0.9$ MK (or $T_{\text{eff}}^{\infty} \simeq 0.7$ MK) and $R \simeq 13$ km (for the estimated distance to the pulsar $D = 300$ pc), respectively. The bolometric luminosity of the thermal emission is $L_{\text{bol}} \simeq 0.8 \times 10^{33}$ ergs s^{-1} . Moreover, the slope of the nonthermal emission depends on the thermal model applied for interpreting the pulsar’s spectrum. It is a rather large photon index $\Gamma \simeq 2.7$ if the blackbody radiation is used. The nonthermal component with this slope greatly exceeds the optical emission of the pulsar. In the analysis involving the atmosphere model the nonthermal component is much flatter, with $\Gamma \simeq 1.5$. Remarkably, the extrapolation of this power-law spectrum (with $L^{\text{nonth}} \simeq 0.2 \times 10^{32}$ ergs s^{-1} , or about 40 times lower than L_{bol}) matches fairly

⁹ The featureless spectrum of Vela obtained with *Chandra* at a high-energy resolution indicate that there are no heavy elements on the pulsar’s surface.

well the optical and hard X-ray/soft γ -ray fluxes detected from the pulsar. This is shown in Figure 7.

The X-ray pulsed profile of Vela is very unusual and complicated, with at least three peaks per rotational period and $f_p \approx 8\%$ (Pavlov, Zavlin & Sanwal 2002). A combined spectral and timing analysis is crucial to further elucidate mechanisms generated X-ray emission of this pulsar.

PSR 1706–44 is one more young and energetic pulsar ($P = 0.102$ s, $\tau_c = 18$ kyr, $\dot{E} = 3.4 \times 10^{36}$ ergs s $^{-1}$) emitting thermal X-rays, with spectral properties very similar to those of Vela (McGowan et al. 2004). The thermal component of PSR 1706–44 detected with *XMM-Newton* can be described by a magnetized hydrogen atmosphere model with $T_{\text{eff}} \simeq 1.0$ MK and $R \simeq 12$ km (for $D = 2.3$ kpc), or $L_{\text{bol}} \simeq 1.0 \times 10^{33}$ ergs s $^{-1}$. The nonthermal emission is fitted with a power-law spectrum of $\Gamma \simeq 1.4$, but its luminosity, $L^{\text{nonth}} \simeq L_{\text{bol}}$, is much higher than that of Vela. The X-ray pulsed profile of PSR 1706–44 is energy-dependent and shows a broad pulse per period with $f_p \approx 10\%$ at energies $E \lesssim 1.4$ keV, where the thermal flux dominates.

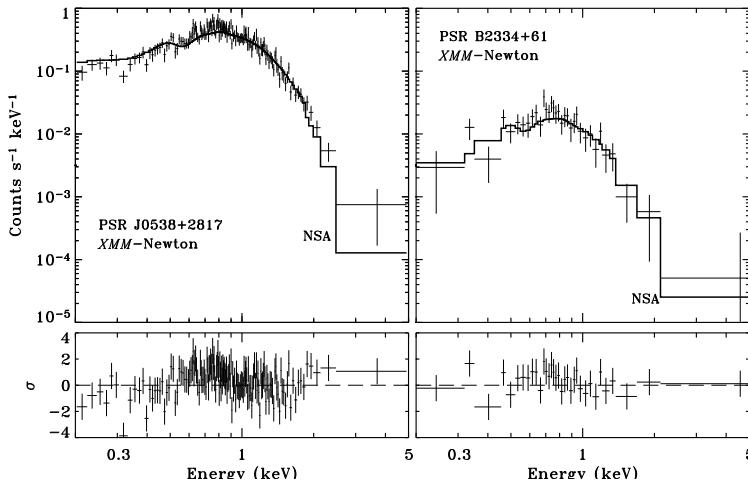


Fig. 8. X-ray spectrum of PSRs J0538+2817 and B2334+61 detected with *XMM-Newton* (crosses) and fitted with magnetized neutron star atmosphere models (see §4.3). Residuals in the fits are shown in the lower panel.

4.3 PSRs J0538+2817 and B2334+61

These two neutron stars have similar pulsar parameters (age, spin period, spin-down power) and could be considered as “twins”, or at least “coevals”, if their ages were derived in the same way.

PSR J0538+2817 ($P = 0.143$ s, $\dot{E} = 4.9 \times 10^{34}$ ergs s $^{-1}$) represents a rare case when neutron star age is well determined. Based on the pulsar’s

proper motion measurements, Kramer et al. (2003) inferred the true age of PSR J0538+2817, $\tau \simeq 30$ kyr, much smaller than the standard estimate $\tau_c = 618$ kyr.

No nonthermal emission was observed from PSR J0538+2817. The pulsar’s spectrum detected with XMM-Newton can be fitted with a single blackbody radiation of $T_{\text{bb}}^\infty \simeq 2.1$ MK and $R_{\text{bb}}^\infty \simeq 1.7$ km for a distance $D = 1.2$ kpc (McGowan et al. 2003). As shown by Zavlin & Pavlov (2004b), a hydrogen atmosphere model with $B = 10^{12}$ G fits the observational data even better, yielding the surface temperature $T_{\text{eff}} \simeq 1.1$ MK and the pulsar radius $R \simeq 10.5$ km (at $M = 1.4M_\odot$), or $L_{\text{bol}} \simeq 1.2 \times 10^{33}$ ergs s^{-1} . An upper limit on luminosity of a possible nonthermal component is $L^{\text{nonth}} < 1.0 \times 10^{31}$ ergs s^{-1} (assuming $\Gamma = 1.5$).

The X-ray flux of PSR J0538+2817 is pulsed, with a broad, asymmetric pulse per period and pulsed fraction $f_p \approx 25\%$. The phases of pulse maxima at energies below and above 0.8 keV differ by $\sim 75^\circ$ (Zavlin & Pavlov 2004b). This indicates that the thermal emission is intrinsically anisotropic and the pulsar has a strong nonuniformity of the surface temperature and magnetic field.

The estimate on the age of PSR B2334+61 ($P = 0.495$ s, $\dot{E} = 6.2 \times 10^{34}$ ergs s^{-1}) is obtained in the standard way, $\tau_c = 41$ kyr. Similar to the case of PSR J0538+2817, the X-ray flux of PSR B2334+61 detected with XMM-Newton if of a thermal origin, and the pulsar’s spectrum can be fitted with a single thermal model (McGowan et al. 2006). The blackbody fit yields $T_{\text{bb}}^\infty \simeq 1.5$ MK and $R_{\text{bb}}^\infty \simeq 2.8$ km for a distance $D = 3.1$ kpc. A hydrogen atmosphere models with $R = 10$ km, $M = 1.4M_\odot$ and $B = 10^{13}$ G fits equally well the observational data, resulting in the surface temperature $T_{\text{eff}} \simeq 0.9$ MK and $L_{\text{bol}} \simeq 0.5 \times 10^{33}$ ergs s^{-1} . A lower limit on luminosity of a possible nonthermal component is $L^{\text{nonth}} < 0.7 \times 10^{31}$ ergs s^{-1} (for $\Gamma = 1.5$). Based on the results of the spectral fits, one can assume that these two pulsars are indeed “twins” and the estimate τ_c on the age of PSR B2334+61 is close to the pulsar’s true age. Figure 8 shows the spectra detected from PSRs J0538+2817 and B2334+61 and fitted with the best neutron star atmosphere models. The only difference in the X-ray properties of these two objects is that the emission observed from PSR B2334+61 revealed no pulsations, with a 5% upper limit on the pulsed fraction, indicating different neutron star geometries of these pulsars (e.g., PSR B2334+61 could have smaller ζ and/or α angles — see Fig. 3).

4.4 Middle-aged pulsars: B0656+14, B1055–52, and Geminga

As discussed in § 2, middle-aged (a few hundred thousand years old) pulsars are believed to be best targets for observing thermal neutron star emission. The well-known three neutron stars with close pulsar parameters, PSRs B0656+14, B1055–52, and Geminga¹⁰, support this. Observations with *ROSAT* first

¹⁰ Dubbed as “Three Musketeers” by Joachim Trümper.

showed that soft X-ray emission from these objects are of a thermal origin (Ögelman 1995), and later *Chandra* and *XMM-Newton* allowed a detailed study of this radiation (Pavlov, Zavlin & Sanwal 2002, Zavlin & Pavlov 2004b, De Luca et al. 2005, Kargaltsev et al. 2005).

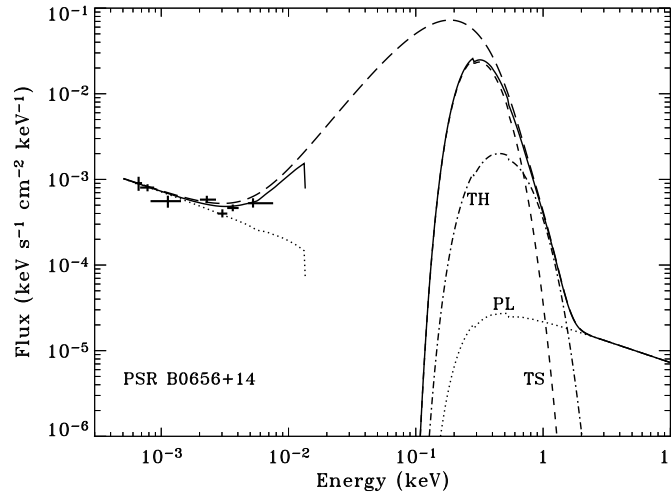


Fig. 9. Broadband spectrum of PSR B0656+14 for a three-component model (TS+TH+PL; see § 4.4) extrapolated in optical. The solid and long-dashed curves show the absorbed and unabsorbed spectra, respectively. Crosses indicate the IR-optical fluxes.

PSR B0656+14 ($P = 0.385$ s, $\tau_c = 111$ kyr, $\dot{E} = 3.8 \times 10^{34}$ ergs s $^{-1}$) is the brightest of these three neutron stars. Its X-ray spectrum cannot be fitted by a two-component model like those describing the spectra of PSRs J1119–6127, B1706–44, and Vela. If fitted with a blackbody radiation, the pulsar’s thermal emission requires two components, a “soft” one (TS) with $T_{\text{bb},s}^\infty \simeq 0.8$ MK and $R_{\text{bb},s}^\infty \simeq 7.5$ km, and a “hard” one (TH) with $T_{\text{bb},s}^\infty \simeq 1.7$ MK and $R_{\text{bb},s}^\infty \simeq 0.6$ km (for $D = 300$ pc). The TS component of the bolometric luminosity $L_{\text{bol},s}^\infty \simeq 1.6 \times 10^{32}$ ergs s $^{-1}$ may be regarded as emitted from the whole pulsar’s surface, whereas the TH component ($L_{\text{bol},s}^\infty \simeq 0.2 \times 10^{32}$ ergs s $^{-1}$) could be interpreted as radiation from heated polar caps. In addition to these two thermal components, a power-law spectrum is needed to fit the pulsar’s emission detected at energies above 2 keV. With the available data, the slope of the nonthermal component is not well constrained, but one can assume that the photon index does not change from optical to X-rays, like in

the Vela pulsar. Then, it results in a power-law spectrum with $\Gamma \simeq 1.5$ and $L^{\text{nonth}} \simeq 0.3 \times 10^{31}$ ergs s^{-1} . Figure 9 presents the broadband emission of PSR B0656+14.

The X-ray spectrum of PSR B1055-52 ($P = 0.197$ s, $\tau_c = 535$ kyr, $\dot{E} = 3.0 \times 10^{34}$ ergs s^{-1}) is very similar to that of PSR B0656+14. It can be fitted only with a three-component model, “soft” and “hard” blackbody radiation plus a power law, with the following parameters (as inferred by Pavlov, Zavlin & Sanwal 2002 from the combined *ROSAT* and *Chandra* data on the pulsar): $T_{\text{bb},s}^\infty \simeq 0.8$ MK and $R_{\text{bb},s}^\infty \simeq 8.4$ km, $T_{\text{bb},s}^\infty \simeq 1.6$ MK and $R_{\text{bb},s}^\infty \simeq 0.6$ km (for $D = 700$ pc), a photon index $\Gamma \simeq 1.7$ and $L^{\text{nonth}} \simeq 0.9 \times 10^{31}$ ergs s^{-1} .

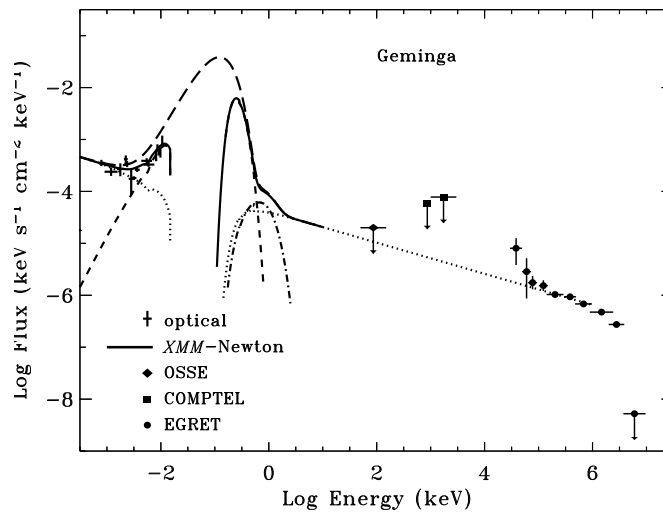


Fig. 10. Multiwavelength spectrum of Geminga observed with different missions. The X-ray flux is described with a three-component (TS+TH+PL) model. The solid and long-dashed curves are the absorbed and unabsorbed fluxes, respectively. Short dashes, dash-dots, and dots show the TS, TH, and PL components, respectively (see §4.4).

Compared to the spectra of PSRs B0656+1 and B1055-52, the X-ray flux of the famous γ -ray and X-ray Geminga pulsar¹¹ ($P = 0.237$ s, $\tau_c = 342$ kyr, $\dot{E} = 3.3 \times 10^{34}$ ergs s^{-1}) alone does not require a three-component model. It can be fitted with two components, a blackbody spectrum and a power law of $\Gamma \simeq 2.0$. However, the nonthermal component extrapolated to low energies greatly exceed optical fluxes observed from the pulsar. To describe

¹¹ Geminga has not been firmly confirmed as a radio pulsar.

the optical/*UV/FUV* and X-ray data with the same model, one needs to invoke a three-component interpretation of the X-ray flux, similar to that applied for the other “Musketees”, with $T_{\text{bb},s}^{\infty} \simeq 0.5$ MK and $R_{\text{bb},s}^{\infty} \simeq 12.9$ km, $T_{\text{bb},s}^{\infty} \simeq 2.3$ MK and $R_{\text{bb},s}^{\infty} \simeq 0.05$ km (for $D = 200$ pc), and a photon index $\Gamma \simeq 1.5$ and $L^{\text{nonth}} \simeq 0.2 \times 10^{31}$ ergs s $^{-1}$ (Kargaltsev et al. 2005). Figure 10 shows the multiwavelength spectrum of Geminga based on this three-component interpretation. It is worthwhile to mention that, although this spectral model is similar to those suggested for the X-ray emission of PSRs B0656+1 and B1055–52, the $R_{\text{bb},h}^{\infty}$ radius inferred for Geminga is smaller by about a factor of 10 than the estimates obtained for the other two pulsars. Note that according to theoretical pulsar models (§ 2) these three objects should have about the same polar cap radii.

Applying magnetized hydrogen atmosphere models for the thermal components observed from all three pulsars yields formally acceptable fits. However, they imply very large radii for the TS component, $R \gtrsim 40$ km. Therefore, applicability of the available neutron star atmosphere models to these objects is questionable.

The pulsations of the X-ray fluxes from these three pulsars shows a complex behavior, with energy-dependent variations in pulsed fraction, phase of main pulses, and pulse shape (Pavlov, Zavlin & Sanwal 2002, Zavlin & Pavlov 2004b, Kargaltsev et al. 2005). This indicates that their thermal radiation is locally anisotropic, in obvious contradiction with the simplistic blackbody interpretation of the phase-integrated spectra. Moreover, the observed pulsed profiles hints that the surface distributions of temperature and magnetic field are not azimuthally symmetric, suggesting a strong multipolar component of the magnetic field or a decentered magnetic dipole.

4.5 Old radio pulsars

Because of their age, $\tau_c > 1$ Myr, old ordinary (with spin periods $P \gtrsim 0.05$ s, i.e., not millisecond) radio pulsars are expected to be and actually are much less energetic and fainter than their younger “stellarmates”. Up to now, of about 1,100 such pulsars known¹², only seven have been firmly detected in X-rays¹³ (Zavlin & Pavlov 2004a, Zhang, Sanwal & Pavlov 2005, Kargaltsev, Pavlov & Garmire 2006). The analysis of X-rays collected from these old neutron stars revealed very diverse properties of their emission, with thermal radiation undoubtedly detected from two objects, PSRs B0950+08 and J2043+2740 (Zavlin & Pavlov 2004a).

¹² According the pulsar catalog provided by the Australia Telescope National Facility; <http://www.atnf.csiro.au/research/pulsar>.

¹³ Marginal X-ray detection of two more old pulsars have been reported (Zavlin & Pavlov 2004a).

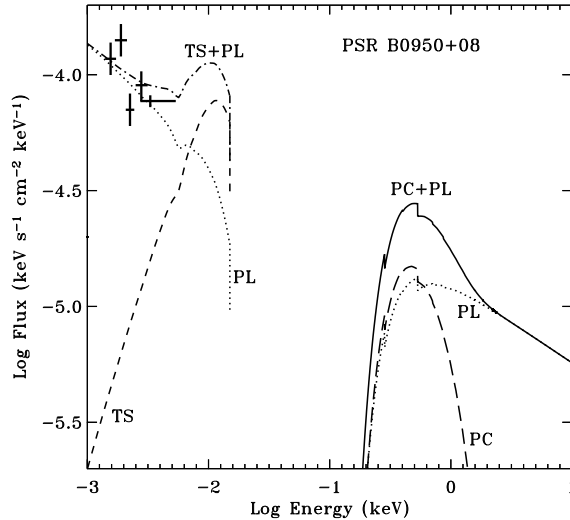


Fig. 11. Broadband spectrum of PSR B0950+08 for a two-component, polar caps (PC) plus power law (PL), model (see § 4.5) extrapolated in optical. Crosses show the optical fluxes. Radiation from the whole surface (TS) is also indicated.

PSR B0950+08

The X-ray spectrum of PSR B0950+08 ($P = 0.253$ s, $\tau_c = 17.4$ Myr, $\dot{E} = 5.6 \times 10^{32}$ ergs s $^{-1}$) detected with *XMM-Newton* is best described with a two-component model, thermal plus nonthermal. The thermal component, dominating at energies $E \lesssim 0.7$ keV, is interpreted as radiation from two heated polar caps on the star's surface covered with a magnetized ($B \approx 3 \times 10^{11}$ G) hydrogen atmosphere. The applied model takes into account the GR effects (redshift and gravitational bending). The inferred temperature, radius, and luminosity of the polar caps are $T_{pc} \simeq 1.0$ MK, $R_{pc} \simeq 0.25$ km, and $L_{bol}^{pc} \simeq 0.3 \times 10^{30}$ ergs s $^{-1}$ (for a distance $D = 260$ pc), respectively. Remarkably, the obtained polar cap radius is in excellent agreement with the conventional estimate $R_{pc}^* \simeq 0.3$ km (§ 2). The nonthermal emission is fitted with a power-law spectrum of a photon index $\Gamma \simeq 1.3$ and luminosity $L^{nonth} \simeq 1.0 \times 10^{30}$ ergs s $^{-1}$. This power-law model also matches well optical fluxes detected from the pulsar. Figure 11 presents the broadband, from optical to X-rays, spectrum of PSR B0950+08. The analysis of the temporal behavior of the pulsar's X-ray flux, with energy-dependent pulse shape and pulsed fraction, also supports this two-component interpretation. The combined optical and X-ray data put the upper limit on the temperature of the bulk of the neutron star surface, $T_{surf} < 0.1$ MK (assuming the standard neutron star radius $R = 10$ km).

PSR J2043+2740

Analysis of the X-ray flux of PSR J2043+2740 ($P = 0.096$ s, $\tau_c = 1.2$ Myr, $\dot{E} = 5.6 \times 10^{34}$ ergs s $^{-1}$) observed with XMM-Newton firmly showed, despite a low number of photons collected, that the pulsar's spectrum is very soft, with no emission detected at energies $E \gtrsim 2$ keV. A single power-law fit to these data yields a photon index $\Gamma \simeq 4.7$, that greatly exceeds a typical value $\Gamma = 1\text{--}2$ found in nonthermal radiation of a large sample of radio pulsars (including the examples discussed in this paper), with ages varying in a broad range, from about 1 kyr to 20 Myr. This fact completely rules out a nonthermal interpretation of the X-ray emission of PSR J2043+2740. Applying blackbody radiation to these X-ray data yields $T_{\text{bb}}^\infty \simeq 0.9$ and $R_{\text{bb}}^\infty \simeq 2.7$ km (for a distance $D = 1.8$ kpc), that could be suggestive that the X-ray emission originates from polar caps. However, this radius estimate is a factor of 5 larger than the theoretical prediction $R_{\text{pc}}^* \simeq 0.5$ km. On the other hand, the fits with magnetized ($B \approx 4 \times 10^{11}$ G) hydrogen atmosphere models gives the surface effective temperature $T_{\text{eff}} \simeq 0.6$ MK for the neutron star radius $R = 9$ km. The latter fit indicates that the detected X-ray emission most likely emerges from the bulk of the star's surface, with the bolometric luminosity $L_{\text{bol}} \simeq 0.8 \times 10^{30}$ ergs s $^{-1}$. This result is rather unexpected because PSR J2043+2740 has the highest spin-down power among all known ordinary pulsars with $\tau_c > 1$ Myr and, hence, it should have been the strongest nonthermal emitter among old ordinary pulsars. Hopefully, someday a longer observation of this pulsar will provide more details on the properties of its thermal X-ray emission.

4.6 Millisecond pulsars

Millisecond pulsars, with unique properties, represent an evolutionarily distinct group among radio pulsars. First of all, they possess very short and stable spin periods, $P \lesssim 0.05$ s with $\dot{P} \lesssim 10^{-18}$ s s $^{-1}$, and low surface magnetic fields, $B \lesssim 10^{10}$ G. They are thought to be extremely old neutron stars ($\tau_c \sim 0.1\text{--}10$ Gyr) presumably spun up by angular momentum transfer in binary systems. X-ray detections have been reported for about 35 (nonaccreting) millisecond pulsars (of more than a hundred currently known). The majority of them are located in the globular cluster 47 Tuc and exhibit thermal X-rays most probably emitted from heated polar caps (Bogdanov et al. 2006). However, detailed spectral and timing information on X-ray emission has been obtained only for eight of the detected millisecond pulsars (see Zavlin 2007 for a review). One half of them are nonthermally emitting pulsars. The bulk of X-rays from the other four objects originates from heated polar caps. These are PSRs J0030+0451, J2124–3358, J1024–0719, and J0437–4715, with similar characteristics of the detected X-ray flux. The latter is the nearest ($D = 140$ pc) and brightest millisecond pulsar, and properties of its X-ray emission are discussed below.

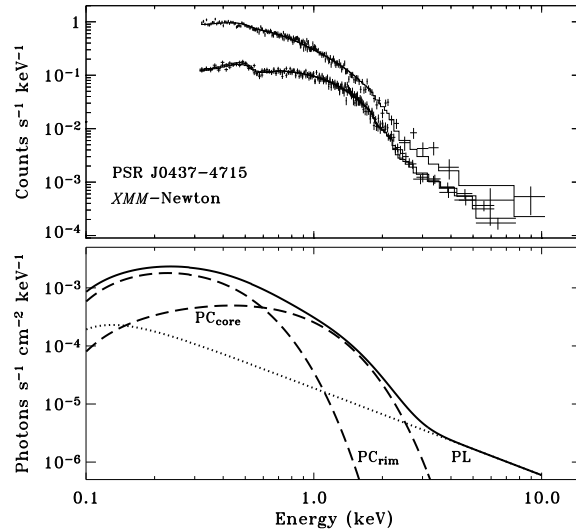


Fig. 12. X-ray spectrum of PSR J0437–4715 detected with different instruments onboard *XMM-Newton* (crosses in the upper panel) and fitted with a composite model, two-temperature (“core” and “rim”) polar caps (PC) and power law (PL), shown in the lower panel (see § 4.6).

PSR J0437–4715

Pulsed X-ray emission from this pulsar ($P = 5.76$ ms, $\tau_c = 6.5$ Gyr, $\dot{E} = 3.8 \times 10^{33}$ ergs s^{-1}) was discovered with *ROSAT* (Becker & Trümper 1993), and observations with *Chandra* and *XMM-Newton* have finally established its properties (Zavlin et al. 2002, Zavlin 2006). The model describing the pulsar’s X-ray flux consists of a thermal and nonthermal components. The thermal component is emitted from two identical polar caps covered with a (nonmagnetic) hydrogen atmosphere and located at the poles of a magnetic dipole. As first proposed by Zavlin & Pavlov (1998), the polar caps of a millisecond pulsar would have a nonuniform temperature because low surface magnetic field does not prevent the energy (heat) released by relativistic particles from propagating along the surface to an area of a radius larger than the conventional estimate R_{pc}^* . The uniform temperature is approximated by a step-function mimicking a smaller and hotter polar cap “core” and a larger and colder “rim”. The GR effects (redshift and gravitational bending) are accounted for in this interpretation. The thermal model, supplemented with a power-law component, fits well the X-ray emission detected from PSR J0437–4715 up to 10 keV and yields reasonable spectral parameters: $T_{pc}^{core} \simeq 1.4$ MK and $T_{pc}^{rim} \simeq 0.5$ MK, $R_{pc}^{core} \simeq 0.4$ km and $R_{pc}^{rim} \simeq 2.6$ km, with the total bolometric luminosity $L_{bol}^{pc} \simeq 1.8 \times 10^{30}$ ergs s^{-1} . The nonthermal component has a photon index $\Gamma \simeq 1.8$ and luminosity $L^{nonth} \simeq 0.5 \times 10^{30}$ ergs s^{-1} . Figure 12 presents this model and the fit to the data on PSR J0437–4715 col-

lected with *XMM-Newton*. Interestingly, PSR J0437–4715 has been detected in *UV/FUV* with *HST* (Kargaltsev, Pavlov & Romani 2004). The shape of the inferred spectrum suggests thermal emission from the whole neutron star surface of a surprisingly high temperature of about 0.1 MK. A powerful energy source (most likely, internal chemical and/or frictional heating) should be operating in a Gyr-old neutron star to keep its surface at such temperature.

X-ray emission from all four thermally emitting millisecond pulsars is pulsed, with pulsed fraction $f_p \simeq 35\%–50\%$ (Zavlin 2007). Such pulsed fraction can be produced only by intrinsically anisotropic radiation, that supports the assumption on presence of a hydrogen atmosphere on the surface of millisecond pulsars. The pulsed profiles of PSRs J0437–4715, J2124–3358, and J1024–0719 are rather similar in shape, with single broad pulses, whereas the light curve of PSR J0030+0451 exhibits two pulses per period indicating that the geometry of this pulsar (the angles ζ and α — see Fig. 3) is different from those of the three others. For example, in the framework of the conventional pulsar model with the magnetic dipole at the neutron star center, PSR J0030+0451 can be a nearly orthogonal rotator (i.e., $\zeta \simeq \alpha \simeq 90^\circ$) with two pulses in its light curve being due to contributions from two polar caps seen during the pulsar’s rotation. For the others, the bulk of the detected X-ray flux is expected to come mostly from one polar cap. Importantly, as first demonstrated by Pavlov & Zavlin (1997) and Zavlin & Pavlov (1998) on the X-ray emission of PSR J0437–4715 detected with *ROSAT*, analyzing pulsed emission with thermal polar cap models can put stringent constraints on the neutron star mass-to-radius ratio M/R if the star’s geometry is known (e.g., from radio polarization data).

4.7 Putative pulsars: CXOU J061705.3+222127 (= J0617) and RX J0007.0+7302 (=J0007)

The compact source J0617 discovered in a short *Chandra* observation (Olbet et al. 2001) is located within a bright X-ray comet-like nebula. Most likely, J0617 is a young, fast and energetic pulsar that powers this nebula. To firmly confirm this very plausible hypothesis, pulsations of emission from this object (in radio and/or X-rays) have to be detected yet. A longer *Chandra* observation of J0617 and the nebula provided more details on X-ray properties of the source and surrounding diffuse emission (Gaensler et al. 2006, Weisskopf et al. 2007). The X-ray spectrum of J0617 reveals a thermal component which dominates at energies $E \lesssim 1.7$ keV. At higher energies, a nonthermal emission prevails. The fact that the spectrum of J0617 is very similar to those found in the young and powerful pulsars, J1119–6127 (§ 4.1), Vela, and B1706–4 (§ 4.2), strongly supports the assumption on this compact source being a neutron star and a pulsar. The detected spectrum can be equally well fitted with both blackbody plus power-law and hydrogen atmosphere plus power-law combinations. Applying magnetized atmosphere models interprets the thermal flux as emitted from the whole neutron surface of $T_{\text{eff}} \simeq 0.8$ MK and radius $R = 10$

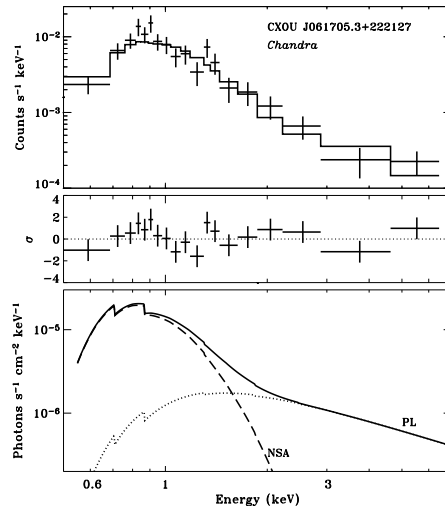


Fig. 13. Two-component, hydrogen magnetized atmosphere (NSA) model plus a power law (PL), fit to the X-ray spectrum of CXOU J061705.3+222127 detected with *Chandra* (upper panel). The middle panel shows residuals in the fit, whereas the lower panel presents the contributions (attenuated by interstellar absorption) from the thermal (dashes) and nonthermal (dots) components (see § 4.7).

km (for a distance $D = 1.5$ kpc), with $L_{\text{bol}} \simeq 2.9 \times 10^{32}$ ergs s^{-1} , and yields the nonthermal spectrum of $\Gamma \simeq 1.2$ with $L^{\text{nonth}} \simeq 0.2 \times 10^{32}$ ergs s^{-1} , about 15 times smaller than the thermal luminosity. The spectrum of J0617 fitted with this two-component model is presented in Figure 13. It should be noted that, like in the case of Vela, using blackbody radiation instead of atmosphere models results in much steeper power-law component of $\Gamma \simeq 2.7$, that is not typical for nonthermal emission from radio pulsars. Hence, the interpretation involving the atmosphere models can be regarded as more preferable.

Another putative pulsar with a possible γ -ray counterpart powering an X-ray nebula is the compact source J0007 at the center of the SNR CTA 1 (but not a CCO discussed in § 4.8). As obtained by Slane et al. (2004b), its X-ray spectrum detected with *XMM-Newton* is well fitted with a magnetized hydrogen atmosphere model of the same parameters as those derived for J0617 (assuming $D = 1.4$ kpc), plus a power-law component of $\Gamma \simeq 1.6$ and $L^{\text{nonth}} \simeq 0.5 \times 10^{32}$ ergs s^{-1} . Extrapolation of this power-law spectrum to high energies is consistent with the flux detected from the proposed γ -ray counterpart, strengthening the proposition that J0007 is a γ -ray emitting pulsar.

4.8 “Pure” thermally emitting neutron stars

All objects presented in §§ 4.1–4.7 are either radio pulsars or show other manifestations of the nonthermal activity. Below I briefly discuss a few examples of radio-quiet neutron stars emitting only thermal X-ray emission.

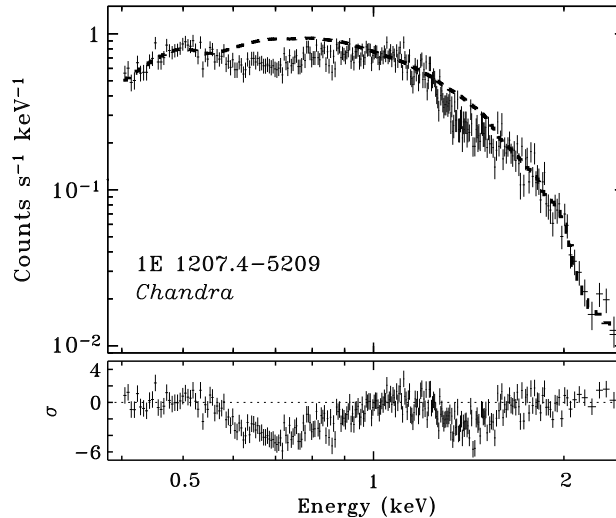


Fig. 14. *Upper panel:* Spectrum of 1E 1207.4–5209 detected with *Chandra* (crosses) vs. a featureless thermal model (dashes). *Lower panel:* Residuals between the observed and model spectra demonstrating the presence of the two absorption features in the X-ray emission of this object (see § 4.8).

1E 1207.4–5209 (= 1E1207) and other CCOs

1E1207 belongs to the small group of currently known seven CCOs in SNRs (see Pavlov, Sanwal & Teter 2004 for a review). One of them, the CCO in the SNR RCW 103, is very outstanding because it shows a highly variable X-ray flux and its emission is presumably powered by accretion from a companion in a close binary system with a ~ 6.5 -hr orbital period. The other six CCOs have not shown any long-term variability of their thermal emission, characterized by blackbody temperatures $T_{\text{bb}}^{\infty} \approx 2\text{--}5$ MK and emitting areas $R_{\text{bb}}^{\infty} \approx 0.3\text{--}3$ km, and seem to be similar to each other. However, the spin periods¹⁴ of two objects, 1E1207 in the SNR PKS 1209–51/52 with $P = 0.424$ s (Zavlin et al. 2000) and CXOU J185238.6+004020 in the SNR Kes 79 with $P = 0.105$ s (Gotthelf, Halpern & Seward 2005), make them distinct from the rest.

¹⁴ Typical for radio pulsars.

1E1207 is even more unique: it is the only known nonaccreting neutron star whose X-ray flux contains two firmly detected spectral features. Figure 14 presents the spectrum of 1E1207 with two absorption lines at about 0.7 and 1.4 keV discovered with *Chandra* (Sanwal et al. 2002). These features cannot be explained as proton or electron cyclotron lines, and current interpretations involve atomic transitions of once-ionized helium in a very strong magnetic field, $B \sim 10^{14}$ G (Sanwal et al. 2002; Pavlov & Bezchastnov 2005), or transitions of helium-like oxygen (or neon) in a weaker field $B \sim 10^{11}$ G (Mori & Hailey 2002). First magnetized oxygen atmosphere models of Mori & Ho (2006) seem to be in apparent qualitative agreement with the X-ray spectrum of 1E1207, although it has to be demonstrated yet whether these models could explain the observational data in the quantitative way. In any case, regardless of what the true origin of these spectral lines is, they make 1E1207 one of the most important objects for astrophysics of neutron stars and physics of superdense matter because it provides an opportunity to measure the gravitational redshift at the neutron star surface and constrain the equation of state of the superdense matter in the neutron star interiors.

“Truly isolated” X-ray emitting neutron stars

The final part of the observational section gives a short description of another small group of very intriguing objects — so-called “dim”¹⁵ or “truly isolated” neutron stars. These objects, seven in total, were discovered with *ROSAT*, and a lot of important information on properties of their X-ray emission provided with *Chandra* and *XMM-Newton* is summarized in the detailed reviews by Haberl (2007) and van Kerkwijk & Kaplan (2007). All seven emit thermal X-ray spectra characterized by temperatures $T_{\text{bb}}^{\infty} \approx 0.7\text{--}1.1$ MK. Faint optical counterparts (with magnitudes $m_B > 25$) were identified for five of them. Four objects have periods in the 3.5–11.4 s range, and spin period candidates in the same range have been proposed for the other three. All this strongly suggests that these objects are neutron stars (and I believe nobody doubts this). Extrapolations of the observed X-ray spectra fitted with a blackbody spectrum to optical strongly underpredict measured optical fluxes (where available; see Pavlov, Zavlin & Sanwal 2002 for examples). None of current neutron star atmosphere models applied to the X-ray spectra of these objects either fits or yields reasonable parameters (generally, the atmosphere models result in unrealistic estimates on the neutron stars size, that in turn leads to a large overestimate of observed optical fluxes — see Pavlov et al. 1996). Timing solutions (spin period derivatives) determined for two objects yield very similar estimates on the stars’ age, $\tau_c \approx 2$ Myr, spin-down power, $E \approx 4 \times 10^{30}$ ergs s^{-2} , and surface magnetic field, $B \approx 3 \times 10^{13}$ G. The low estimates derived

¹⁵ As discussed at the “*Isolated Neutron Stars: from the Interior to the Surface*” conference held in April 2006 in London (UK), the historical name “dim” is rather inappropriate because some of these objects are very bright X-ray emitters.

on \dot{E} can explain the absence of nonthermal activity of these two (and, by analogy, all other five) neutron stars. Broad absorption features centered at energies in the 0.3–0.8 keV range have been detected in the radiation of six objects, whereas the seventh one reveals almost a “perfect” blackbody spectrum (Pavlov, Zavlin & Sanwal 2002). What produces the absorption features in the X-ray spectra of six objects is a matter of debate: they might be caused by proton cyclotron resonance in a magnetic field $B \gtrsim 5 \times 10^{13}$ G or produced by atomic transitions in, for example, a strongly magnetized hydrogen surface (if it is in the gaseous state). Any of these hypotheses should be taken with caution until reliable models of surface emission are proposed for these neutron stars. In this respect, the model by Pérez-Azorin et al. (2006) invoking emission from a nonuniform, strongly magnetized and condensed neutron star surface seems to be the most advanced and self-consistent approach to explain emission properties of these objects. There are other intriguing details on properties of these objects (e.g., a long-term variability of the spectral shape of X-ray flux detected from one of them, presumably caused by a neutron star precession) that can be found in the above-mentioned reviews.

5 Concluding remarks

I would like to complete this review with a brief discussion on what has been learned during the extensive, 15-year-long studying of thermal emission from isolated neutron stars.

Undoubtedly, a substantial progress has been made on the theoretical front. Best investigated models are nonmagnetic atmospheres of various chemical compositions and magnetized fully-ionized hydrogen atmospheres. These models have been successfully applied to interpretation of thermal emission to a number of neutron stars, mainly, radio pulsars of different ages, including millisecond pulsars, and yielded reasonable neutron star parameters (surface temperatures and radii of emitting areas). Besides the active pulsars, there is a group of neutron stars transiently accreting in X-ray binaries (e.g., Aquila X-1, KS 1731–260, Centaurus X-4, 4U 1608–522, MXB 1659–29, 4U 2129+47) whose X-ray emission in quiescence has been analyzed with use of the atmosphere models (Rutledge et al. 1999, 2001a,b and 2002, Nowak, Heinz & Begelman 2002, Wijnands et al. 2002 and 2003, Heinke et al. 2006). Although these objects are not isolated, their quiescent radiation is interpreted as emitted from the whole neutron stars surface covered with a nonmagnetic hydrogen atmosphere heated by energy released in pycnonuclear reactions of the compressed accreted material. Importantly, based on the results obtained on the thermal emission from these objects, Yakovlev, Levenfish & Haensel (2003) proposed a new method for studying neutron stars internal structure and equation of state of the inner matter. In addition, as suggested by Rutledge et al. (2000), the atmosphere models can be useful for distinguishing between transiently accreting neutron stars and black holes, in quiescence. First steps

have been undertaken in modeling partially ionized atmosphere models with strong magnetic fields and different chemical compositions, as well as in modeling thermal emission from condensed neutron star surfaces, although both these types of models are still awaiting application to observational data.

Despite a lot of interesting and encouraging results obtained in the thermal emission modeling and with applying these models to observational data, a number of problems remains to be solved. First of all, the approach based on two polarization modes currently used in magnetized atmosphere models is in fact inaccurate and inapplicable for a partially ionized plasma. To construct more advanced models, the problem of radiative transfer in strongly magnetized plasmas should be solved in terms of the four Stokes parameters, with use of the polarizability tensor constructed with aid of the Kramers-Kronig relations (Bulik & Pavlov 1995, Potekhin et al. 2004). Next, investigations of the structure of various atoms, molecules, and molecular chains in strong magnetic fields, as well as radiative transitions in these species (Pavlov 1998), are necessary to construct, in combination with the advanced radiative transfer approach, magnetized atmosphere models of a next generation for different chemical compositions. Very interesting and important are the (virtually unknown) radiative properties of matter in superstrong magnetic fields, $B \gtrsim 10^{14}$ G, apparently found in AXPs and SGRs. More reliable models are required for radiative properties of nonideal plasmas and condensed matter, as well as further investigations of phase transitions between different states of matter in strong magnetic fields.

Not only the models of neutron star atmospheres and condensed surfaces require improvements. Analysis of observational data on thermal flux from neutron stars, especially temporal behavior of detected X-ray emission, shows that the idealized picture of a neutron star with a centered magnetic dipole and uniform surface temperature is oversimplification. Therefore, future computations of thermal emission from a neutron star applied to observational data should use realistic surface temperature distributions to reproduce *both spectral and temporal* properties of observed emission. In particular, the problem of temperature distribution over heated polar caps of millisecond pulsars is of a special importance because modeling pulsed thermal emission from these objects is a promising way to constrain neutron star mass-to radius ratio. For that, more elaborated models of magnetospheric pulsed emission are required to disentangle nonthermal and thermal components.

Confronting the surface temperatures derived from observation data with theoretical models of neutron star thermal evolution (Yakovlev et al. 2005) indicates that the neutron star interiors are most probably superfluid and that these objects may have different masses (e.g., $M \simeq 1.47M_{\odot}$ for Vela and Geminga, and $M \simeq 1.35M_{\odot}$ for PSR B1055–52). But these results are quite uncertain because, first of all, they are based on the assumption that the characteristic age of a neutron star is its true age (see the example of PSR J0538+2817 in §4.3). Next, more importantly, thermal emission mechanisms operating in neutron stars are not completely understood yet,

especially in colder objects. Only rather simple conclusions could be drawn from the obtained results. It looks plausible that younger and hotter objects (this $\tau \simeq \tau_c \lesssim 50$ kyr and $T_{\text{surf}} \gtrsim 1$ MK) are indeed covered with a gaseous atmosphere, strongly ionized if comprised of hydrogen, as suggested by the examples discussed in §§ 4.1–4.3 and (probably) 4.7. To explain why the simple blackbody model fits well thermal radiation from colder neutron stars with strong magnetic fields, whereas atmosphere models do not provide reasonable parameters (§ 4.4), one may suggest that cooling hydrogen-depleted neutron star envelopes undergo a phase transition, forming a condensed surface. But this assumption is challenged by very complicated temporal behavior of the thermal flux detected from many these objects — it can be hardly explained without invoking a strong anisotropy of surface radiation similar to that characteristic to the atmospheric radiation. Therefore, the parameters inferred from the blackbody spectral fits should be taken with caution. It also concerns the two-blackbody (“soft” and “hard”) model suggested for the thermal phase-integrated spectra of the middle-aged pulsars (§ 4.4). It is not clear whether the harder thermal component is real or it emerges because the simplified spectral models were used (e.g., this component is not required in the interpretation involving a power-law spectrum with a phase-dependent photon index — see Jackson & Halpern 2006).

There are even much more unanswered questions related to thermal radiation of neutron stars (concerning, for example, the nature of CCOs and connection between them and other types of neutron stars, the origin of spectral lines in thermal emission of seven objects and why no features are present in spectra of other neutron stars with similar temperatures and magnetic field, etc.) To answer these questions, not only improved models are necessary but also a larger sample of neutron stars of various types observed in different energy ranges, from optical/UV to X-rays, is required. In particular, as shown by Kargaltsev et al. (2005) and Kargaltsev & Pavlov (2007), the *UV/FUV* range is very important for elucidating properties of thermal emission emerging from the whole neutron star surface. Contrary to the X-ray (Wien) part of the thermal emission whose shape is strongly affected by surface chemical composition and temperature inhomogeneties, the *UV/FUV* (Rayleigh-Jeans) tail, proportional to the product $[T_{\text{surf}}R^2]$, can put tight constraints on the surface temperature. Hopefully (“the hope dies last”) enough observational time will be allocated in future for studying these enigmatic objects, neutron stars.

Acknowledgement. The author gratefully acknowledges the collaboration with George Pavlov and many other colleagues in studying neutron stars during the last 15 years and thanks the Heraeus Stiftung and the Physikzentrum Bad Honnef for support and hospitality. The author’s work at the NASA MSFC is supported by a NASA Associateship Award.

References

1. C. Alcock, A.F. Illarionov: *ApJ*, **235**, 534 (1980)
2. W. Becker, J. Trümper: *Nature*, **365**, 528 (1993)
3. W. Becker, G.G. Pavlov: in *The Century of Space Science*, ed. J.A.M. Bleeker, J. Giess, M.C.E. Huber (Dordrecht: Kluwer, 200f1), p. 721
4. W. Becker, B. Aschenbach: in *Neutron Stars, Pulsars, and Supernova Remnants*, ed. W. Becker, H. Lesch, J. Trümper (MPE Report 278, 2002), p. 64
5. V.G. Bezchastnov, G.G. Pavlov, Yu.A. Shibanov, V.E. Zavlin: in *Gamma-ray Bursts*, ed. C. Kouveliotou, M. Briggs, G.J. Fishman, AIP Conf. Proc. 384, (NY: Woodbury, 1996), p. 907
6. S. Bogdanov, J.E. Grindlay, C.O. Heike, F. Camilo, P.C.C. Freire, et al.: *ApJ*, **646**, 1104 (2006)
7. T. Bulik, G.G. Pavlov: *ApJ*, **469**, 373 (1995)
8. P. Chang, L. Bildsten: *ApJ*, **605**, 830 (2004)
9. H.-Y. Chiu, E.E. Salpeter: *Phys. Rev. Lett.*, **12**, 413 (1964)
10. A. De Luca, P.A. Caraveo, S. Mereghetti, M. Negroni, G.F. Bignami: *ApJ*, **623**, 1051 (2005)
11. B.M. Gaensler, S. Chatterjee, P.O. Slane, E. van Swalw, F. Camilo, et al.: *ApJ*, **648**, 1037 (2006)
12. B.T. Gänsicke, T.M. Braje, R.W. Romani: *A&A*, **386**, 1001 (2002)
13. Yu.N. Gnedin, G.G. Pavlov: *JETP*, **38**, 903 (1974)
14. M.E. Gonzalez, V.M. Kaspi, F. Camilo, B.M. Gaensler, M.J. Pivovarov: *ApJ*, **630**, 489 (2005)
15. E.V. Gotthelf, J.P. Halpern, F.D. Seward: *ApJ*, **627**, 390 (2005)
16. G. Greenstein, G.J. Hartke: *ApJ*, **271**, 283 (1983)
17. F. Haberl: in *Isolated Neutron Stars: from the Interior to the Surface*, ed. S. Zane, R. Turolla, D. Page, *Ap&SS*, in press (2007; astro-ps/0609066)
18. J.P. Halpern, S.S. Holt: *Nature*, **357**, 222 (1992)
19. C.O. Heinke, G.B. Rybicki, R. Narayan, J.E. Grindlay: *ApJ*, **664**, 1090 (2006)
20. A. Hewish, S.J. Bell, J.D. Pilkington, P.F. Scott, R.A. Collins: *Nature*, **217**, 709 (1968)
21. W.C.G. Ho, D. Lai: *MNRAS*, **327**, 1081 (2001)
22. W.C.G. Ho, D. Lai: *MNRAS*, **338**, 233 (2003)
23. W.C.G. Ho, D. Lai, A.Y. Potekhin, G. Chabrier: *ApJ*, **599**, 1293 (2003)
24. M.S. Jackson, J.P. Halpern: *ApJ*, **633**, 1114 (2006)
25. A.D. Kaminker, G.G. Pavlov, Yu.A. Shibanov: *Ap&SS*, **86**, 249 (1982)
26. O.Y. Kargaltsev, G.G. Pavlov, R.W. Romani: *ApJ*, **602**, 327 (2004)
27. O.Y. Kargaltsev, G.G. Pavlov, V.E. Zavlin, R.W. Romani: *ApJ*, **625**, 307 (2005)
28. O.Y. Kargaltsev, G.G. Pavlov, G.P. Garmire: *ApJ*, **636**, 406 (2006)
29. O.Y. Kargaltsev, G.G. Pavlov: in *Isolated Neutron Stars: from the Interior to the Surface*, ed. S. Zane, R. Turolla, D. Page, *Ap&SS*, in press (2007; astro-ps/0609656)
30. V.M. Kaspi: in *Young Neutron Stars and Their Environments*, ed. F. Camilo, B.M. Gaensler, IAU Symp. 218 (San Francisco: ASP, 2004), p. 231
31. V.M. Kaspi: in *Isolated Neutron Stars: from the Interior to the Surface*, ed. S. Zane, R. Turolla, D. Page, *Ap&SS*, in press (2007; astro-ps/0610304)
32. V.M. Kaspi, M.S.E. Roberts, A.K. Harding: in *Compact Stellar X-ray Sources*, ed. W.H.G. Lewin, M. van der Klis (Cambridge University Press, 2006), p. 279

33. M. Kramer, A.G. Lyne, G. Hobbs, O. Löhmer, P. Carr, et al.: ApJ, **593**, L31
34. D. Lai, E.E. Salpeter: ApJ, **491**, 270 (1997)
35. K.E. McGowan, J.A. Kennea, S. Zane, F.A. Córdova, M. Cropper, et al.: ApJ, **591**, 380 (2003)
36. K.E. McGowan, S. Zane, M. Cropper, J.A. Kennea, F.A. Córdova, et al.: ApJ, **600**, 343 (2004)
37. K.E. McGowan, S. Zane, M. Cropper, W.T. Vestrand, C. Ho: ApJ, **639**, 377 (2006)
38. S. Mereghetti, L. Chiarlone, G.L. Israel, L. Stella: in *Neutron Stars, Pulsars, and Supernova Remnants*, ed. W. Becker, H. Lesch, J. Trümper (MPE Report 278, 2002), p. 29
39. K. Mori, C.J. Hailey: ApJ, **564**, 914 (2002)
40. K. Mori, C.J. Hailey: ApJ, **648**, 1139 (2006)
41. K. Mori, W.C.G. Ho: MNRAS, submitted, (2006; astro-ph/0611145)
42. M.A. Nowak, S. Heinz, M.C. Begelman: ApJ, **573**, 778 (2002)
43. H. Ögelamm: in *The Lives of neutron Stars*, ed. A. Alpar, U. Kilizóglu, J. van Paradijs (Dordrecht: Kluwer, 1995), p. 101
44. C.M. Olbert, C.R. Clearfield, N.E. Williams, J.W. Keohane, D.A. Frail: ApJ, **554**, L205 (2001)
45. F. Özel: ApJ, **563**, 276 (2001)
46. G.G. Pavlov, Yu.N. Gnedin: Astr. Space Phys. Rev., **3**, 197 (1984)
47. G.G. Pavlov, P. Mészáros: ApJ, **416**, 752 (1993)
48. G.G. Pavlov, Yu.A. Shibano, J. Ventura, V.E. Zavlin: A&A, **289**, 847 (1994)
49. G.G. Pavlov, Y.A. Potekhin: ApJ, **450**, 883 (1995)
50. G.G. Pavlov, Yu.A. Shibano, V.E. Zavlin, R.D. Meyer: in *The Lives of neutron Stars*, ed. A. Alpar, U. Kilizóglu, J. van Paradijs (Dordrecht: Kluwer, 1995), p. 71
51. G.G. Pavlov, V.E. Zavlin, J. Trümper, R. Neuhauser: ApJ, **472**, L33 (1996)
52. G.G. Pavlov, V.E. Zavlin: ApJ, **490**, L91 (1997)
53. G.G. Pavlov: in *Atoms and Molecules in Strong External Fields*, ed. P. Schmelcher, W. Schweizer (New York : Plenum, 1998), p. 37
54. G.G. Pavlov, V.E. Zavlin: in *Highly Energetic Physical Processes and Mechanisms for Emission from Astrophysical Plasmas*, ed. P.C.H. Martens, S. Tsuruta, M.A. Weber (PASP: IAU Symp. 195, 2000a), p. 103
55. G.G. Pavlov, V.E. Zavlin: ApJ, **529**, 1011 (2000b)
56. G.G. Pavlov, V.E. Zavlin, D. Sanwal, V. Burwitz, G.P. Garmire: ApJ, **552**, L129 (2001)
57. G.G. Pavlov, D. Sanwal, G.P. Garmire, V.E. Zavlin: in *Neutron Stars in Supernova Remnant*, ed. P.O. Slane, B.M. Gaensler (San Francisco: ASP, 2002), p. 247
58. G.G. Pavlov, V.E. Zavlin, D. Sanwal: in *Neutron Stars, Pulsars, and Supernova Remnants*, ed. W. Becker, H. Lesch, J. Trümper (MPE Report 278, 2002), p. 273
59. G.G. Pavlov, D. Sanwal, M.A. Teter: in *Young Neutron Stars and Their Environments*, ed. F. Camilo, B.M. Gaensler, IAU Symp. 218 (San Francisco: ASP, 2004), p. 239
60. G.G. Pavlov, V.G. Bezchastnov: ApJ, **635**, L61 (2005)
61. K.R. Pechenick, C. Ftaclas, J.M. Cohen: ApJ, **274**, 846 (1983)
62. J.F. Pérez-Azorin, J.A. Pons, J.A. Miralles, G. Miniutti: A&A, **459**, 175 (2006)

63. J.A. Pons, F.M. Walter, J.M. Lattimer, M. Prakash, R. Neuhäuser: ApJ, **564**, 981 (2002)
64. A.Y. Potekhin, D. Lai, G. Chabrier, W.C.G. Ho: ApJ, **612**, 1034 (2004)
65. M. Rajagopal, R.W. Romani: ApJ, **461**, 327 (1996)
66. M. Rajagopal, R.W. Romani, M.C. Miller: ApJ, **479**, 347 (1997)
67. R.W. Romani: ApJ, **313**, 718 (1987)
68. R.E. Rutledge, L. Bildsten, E.F. Brown, G.G. Pavlov, V.E. Zavlin: ApJ, **514**, 945 (1999)
69. R.E. Rutledge, L. Bildsten, E.F. Brown, G.G. Pavlov, V.E. Zavlin: ApJ, **529**, 985 (2000)
70. R.E. Rutledge, L. Bildsten, E.F. Brown, G.G. Pavlov, V.E. Zavlin: ApJ, **551**, 921 (2001a)
71. R.E. Rutledge, L. Bildsten, E.F. Brown, G.G. Pavlov, V.E. Zavlin: ApJ, **559**, 1054 (2001b)
72. R.E. Rutledge, L. Bildsten, E.F. Brown, G.G. Pavlov, V.E. Zavlin, et al.: ApJ, **580**, 413 (2002)
73. D. Sanwal, G.G. Pavlov, V.E. Zavlin, M.A. Teter: ApJ, **574**, L61 (2002)
74. S. Shapiro, S. Teukolsky: *Black Holes, White Dwarfs, and Neutron Stars*, (New York: Wiley, 1983)
75. Yu.A. Shibano, V.E. Zavlin, G.G. Pavlov, J. Ventura: A&A, **266**, 313 (1992)
76. Yu.A. Shibano, V.E. Zavlin: Astron. Lett., **21**, 3 (1995)
77. P. Slane, D.J. Helfand, E. van der Swaluw, S.S. Murray: ApJ, **616**, 403 (2004a)
78. P. Slane, E.R. Zimmerman, J.P. Hughes, F.D. Seward, B.M. Gaensler, et al.: ApJ, **601**, 1045 (2004b)
79. A.F. Tennant, W. Becker, M. Juda, R.F. Elsner, J.J. Kolodziejczak, et al.: ApJ, **554**, 173 (2001)
80. S. Tsuruta: Ph.D. Thesis (New York: Columbia University, 1964)
81. R. Turolla, S. Zane, J.J. Drake: ApJ, **603**, 265 (2004)
82. M. van Adelsberg, D. Lai, A.Y. Potekhin, P. Arras: ApJ, **628**, 902 (2005)
83. M.H. van Kerkwijk, D.L. Kaplan: in *Isolated Neutron Stars: from the Interior to the Surface*, ed. S. Zane, R. Turolla, D. Page, Ap&SS, in press (2007; astro-ps/0607320)
84. M.C. Weisskopf, M. Karovska, G.G. Pavlov, V.E. Zavlin, T. Clarke: in *Isolated Neutron Stars: from the Interior to the Surface*, ed. S. Zane, R. Turolla, D. Page, Ap&SS, in press (2007; astro-ps/0606732)
85. K. Werner, J. Deetjen: in *Pulsar Astronomy — 2000 and Beyond*, ed. M. Kramer, N. Wex, R. Wielebinski (ASP Conf. Ser. 202, 2000), p. 623
86. R. Wijnands, G. Matteo, M. van der Klis, M. Mendez: ApJ, **573**, L45 (2002)
87. R. Wijnands, M. Nowak, J.M. Miller, J. Homan, S. Wachter, et al.: ApJ, **594**, 952 (2003)
88. D.G. Yakovlev, K.P. Levenfish, P. Haensel: A&A, **407**, 265 (2003)
89. D.G. Yakovlev, O.Y. Gnedin, M.E. Gusakov, A.D. Kaminker, K.P. Levenfish, et al.: Nuc. Phys. A, **752**, 590 (2005)
90. S. Zane, R. Turolla, L. Stella, A. Treves: ApJ, **560**, 384 (2001)
91. V.E. Zavlin, Yu.A. Shibano, G.G. Pavlov: Astron. Lett., **21**, 149 (1995)
92. V.E. Zavlin, G.G. Pavlov, Yu.A. Shibano, J. Ventura: A&A, **297**, 441 (1995)
93. V.E. Zavlin, G.G. Pavlov, Yu.A. Shibano: A&A, **315**, 141 (1996)
94. V.E. Zavlin, G.G. Pavlov, Yu.A. Shibano, F.J. Rogers, C.A. Iglesias: in *Röntgenstrahlung from the Universe*, ed. H.-U. Zimmermann, J. Trümper, H. Yorke (MPE Report 263, 1996), p. 209

95. V.E. Zavlin, G.G. Pavlov: *A&A*, **329**, 583 (1998)
96. V.E. Zavlin, G.G. Pavlov, D. Sanwal, J. Trümper: *ApJ*, **540**, L25 (2000)
97. V.E. Zavlin, G.G. Pavlov: in *Neutron Stars, Pulsars, and Supernova Remnants*, ed. W. Becker, H. Lesch, J. Trümper (MPE Report 278, 2002), p. 263
98. V.E. Zavlin, G.G. Pavlov, D. Sanwal, R.N. Manchester, J. Trümper, et al.: *ApJ*, **569**, 894 (2002)
99. V.E. Zavlin, G.G. Pavlov: *ApJ*, **616**, 452 (2004a)
100. V.E. Zavlin, G.G. Pavlov: *Mem.S.A.It.*, **75**, 458 (2004b)
101. V.E. Zavlin: *ApJ*, **638**, 951 (2006)
102. V.E. Zavlin: in *Isolated Neutron Stars: from the Interior to the Surface*, ed. S. Zane, R. Turolla, D. Page, *Ap&SS*, in press (2007; astro-ps/0608210)
103. B. Zhang, D. Sanwal, G.G. Pavlov: *ApJ*, textbf624, L109 (2005)